



Evaluation of the sensitivity of meteorological drought in the Mediterranean region to different data record lengths

Ali Demir Keskiner · Oguz Simsek

Received: 19 December 2023 / Accepted: 17 May 2024 / Published online: 8 June 2024
© The Author(s), under exclusive licence to Springer Nature Switzerland AG 2024

Abstract The division and evaluation of data series used in monitoring drought into different time intervals is a practical approach to detecting the spatial and temporal extent of drought spread. This study aimed to determine meteorological drought's spatial and temporal distribution using overlapping and consecutive periods and cycles of the standardized precipitation index (SPI) time series in the Mediterranean region, Turkey. In the scope of the research, SPI values for the SPI12, SPI6 (1), and SPI6 (2) seasons were calculated for consecutive and overlapping hydrological years (1978–1998/21 years, 1978–2008/31 years, and 1978–2018/41 years) at 28 meteorological stations. Autocorrelation, Mann–Kendall, and Sen slope trend tests were applied at a 5% significance level for each season (SPI12, SPI6 (1), and SPI6 (2)) and different time scales (21, 31, and 41 years). For each season and period, maps of the SPI drought class, average formation of drought class, Mann–Kendall (MK) trend, and Sen's slope (SS) trend test statistics for the Mediterranean region were obtained, and the spatial distribution rate of

trends was determined by drawing hypsometric curves. Changes in drought occurrence at different time scales were thoroughly evaluated with the changing length of data recording. Consequently, it was determined that the mild wet (MIW) and mild drought (MID) classes dominate the study area in the Mediterranean region. Significant and nonstationary changes detected in extreme wet and drought occurrences (extreme wet, EW; severe wet, SW; extreme drought, ED; severe drought, SD) were found to pose a risk in the study area. It was observed that there were spatially and temporally insignificant decreasing drought trends in the Mediterranean basin, considering that the time scales of these trends slowed down. Despite a nonsignificant trend from the MID drought class to the MIW drought class, it is predicted that the MIW and MID classes will maintain their dominance in the Mediterranean region. The central part of the study area (central Mediterranean basin) is the region with the highest drought risk.

Keywords Data record length · Meteorological drought · Mediterranean region · Trend analysis · Spatiotemporal analysis

A. D. Keskiner
Department of Agricultural Structures and Irrigation,
Faculty of Agriculture, Harran University,
Sanliurfa 63050, Türkiye

O. Simsek (✉)
Department of Civil Engineering, Engineering Faculty,
Harran University, Sanliurfa 63050, Türkiye
e-mail: oguzsimsek@harran.edu.tr

Introduction

The fact that events such as drought, increasing temperatures, heat waves, floods, hurricanes, and melting of glaciers caused by global warming are felt more

intensely every day is a critical factor in keeping the studies on this issue up to date. This situation, which concerns the whole world, is a considerable indicator of the necessity of international measures and protocols as well as national-scale planning against global warming (IPCC Report 2020). Due to rising temperatures and changing drought conditions, the risk of drought has increased in some regions, while in others, there is an elevated risk of disasters such as floods and inundations (Hirabayashi et al., 2010; Mujumdar et al., 2020; Nan et al., 2011). Under current conditions, the adverse effects of disasters, which impact all living beings, must be minimized to ensure the sustainability of a healthy ecological environment and the continuity of life.

Drought is a disaster that varies by location and time, is influenced by various parameters, has unpredictable impact levels when it occurs, and has an unknown start and end time (Haile et al., 2019; Kiem et al., 2016). Most importantly, the inability to predict how long the effects of drought will persist in a particular region is a significant challenge. In addition to unfolding gradually, this disaster progresses slowly, expanding its impact area (Tallaksen & Van Lanen, 2004; Wilhite, 2016). Assessing drought, a consequence of changing drought parameters, and determining the levels and priorities of measures are highly complex tasks. Drought is generally classified as meteorological, hydrological, or agricultural, depending on precipitation, runoff, and soil moisture parameters. Meteorological drought, a lack of precipitation (falling below the long-term average), is also seen as the onset of hydrological and agricultural drought (Wang et al., 2016; Dai et al., 2022). Considering this definition, the majority of studies have focused on meteorological drought. Different researchers have proposed various drought assessment methods for evaluating this type of drought. The standardized precipitation index (SPI) method, which is the most common and requires less data than other methods, stands out in the analysis of drought in different regions (Amiri & Gocic, 2023; Dukat et al., 2022; Hinis et al., 2023; Tsesmelis et al., 2023). Patel et al. (2007) conducted a drought analysis using the SPI method with monthly rainfall data measured over 22 years at 160 stations in the Gujarat region of India. It was found that a 3-month SPI time series could be used to determine the region's drought risk. Karavitis et al. (2011) used the SPI to analyze drought in the entire province of Greece, utilizing rainfall data

measured over many years at 46 precipitation observation stations. Karimi et al. (2019) evaluated meteorological drought using the SPI method with 27 years of flow data from numerous stations in Iran at different time scales. Singh et al. (2022) used the SPI method to spatially and temporally analyze drought in southern Bihar, emphasizing the higher likelihood of agricultural drought than other types of drought. Dikici (2020) examined drought in the Asi River Basin using three other drought index methods, including the SPI method for various periods. Using the SPI method, Gumus et al. (2021) analyzed drought in Turkey's southeastern Anatolian Project (GAP) region at 3-, 6-, and 12-month periods. Simsek et al. (2023) investigated meteorological drought in Turkey's Black Sea region using the SPI and RDI methods, revealing the relationship between the results of the two different drought analysis methods. They noted that the SPI method produced acceptable estimates with less data in drought analysis. Alsenjar et al. (2022) analyzed drought in the Black Sea region using precipitation records obtained from 28 meteorological observation stations with the SPI and standardized precipitation evapotranspiration index (SPEI) methods. They emphasized that these two drought methods yielded very similar results. In recent years, studies comparing other meteorological drought index methods that use temperature or potential evapotranspiration values as input alongside precipitation parameters with the SPI method have been frequently conducted. The general evaluation of these studies suggests that the SPI method provides satisfactory results in meteorological drought analysis compared to other drought analysis methods. Many studies have concluded that there is no objection to using the SPI method for drought analysis due to its advantages, such as ease of calculation and the requirement for less data (Berhail & Katipoğlu, 2023; Caloiero, 2017; Simsek et al., 2023).

Trend methods such as the Mann–Kendall (MK) method, innovative trend analysis (ITA), innovative polygon trend analysis (IPTA), and Spearman's rho (SR) method are widely used to detect trends of time series such as meteorological drought. The Mann–Kendall (MK) method is a trend analysis method that has been used for many years. This non-parametric method determines statistically significant trends at different confidence levels in a time series (Citakoglu & Minarecioglu, 2021; Minarecioglu & Çitakoğlu, 2019). Before applying the MK test to a

time series, controlling for serial correlation effects and removing serial correlation from the time series is crucial (Modarres et al., 2016; Wu et al., 2007; Ye et al., 2019). Furthermore, while this method allows for a comprehensive analysis of trends across the entire time series, techniques such as the ITA evaluate trend formation in time series values of different magnitudes (Esit, 2023; Esit et al., 2023b). The MK method has been preferred and utilized in many studies to determine the trend in SPI time series (Achite et al., 2022; Citakoglu & Coşkun, 2022; Gumus et al., 2021, 2022a). In addition to the MK method, the non-parametric Sen's slope (SS) method provides information about the magnitude and trend in time series using a linear model (Buyukyildiz, 2022; Esit et al., 2023c). The MK test and Sen's slope method were then used in the SPI time series to calculate the trend and trend magnitude of meteorological drought in the region (Achite et al., 2023; Esit et al., 2023a; Sharafi et al., 2022). These recent studies show that the MK test and SS method are widely applied to SPI time series for trend analysis.

In the Mediterranean basin, the frequency of heat-waves has been increasing due to climate change (Kuba et al., 2016; Oguz & Akin, 2019). This increase has resulted in a decline in both the quantity and quality of water (Basakin et al., 2019; Saris, 2021), reduced precipitation, and an elevation in annual temperatures, leading to a rise in the frequency and magnitude of natural disasters. Consequently, adverse event occurrences are frequently experienced in the Mediterranean region. The meteorological drought studies in the Mediterranean region, reported as the most sensitive region to ocean oscillations and global warming, are essential for water source planners and management (Bayer Altin & Altin, 2021; Ozturk et al., 2015).

Turkey, characterized by a semiarid climate in the Eastern Mediterranean basin, is positioned among the countries most vulnerable to the adverse effects of climate change (Barriopedro et al., 2011; Giorgi, 2006; Schär et al., 2004). The Mediterranean region, one of the seven regions of Turkey, forms the southern coast. The region's significant production of agricultural products, mainly the export of products, has contributed to the country's economy. A large portion of these products is cultivated in greenhouses. The prevalence of facilities operating for tourism along the Mediterranean coast also emphasizes the

importance of evaluating drought in this region. Moreover, it is noted that this region, reported to be the most sensitive in terms of air currents and drought change in Turkey, is significant (Carter et al., 1972; Dikici, 2020; Turkes, 2020). Drought vulnerability is multidimensional, spatial, and temporal in nature. Therefore, determining the spatial and temporal character, trend, and magnitude of drought in the Mediterranean region is crucial for water resource management and risk sharing. The division and evaluation of data series used in monitoring drought into different time intervals is a practical approach to detecting the spatial and temporal extent of drought spread (Keskiner & Cetin, 2023). Hence, spatial-temporal trends and magnitudes in the datasets are presented spatially at different time scales, and such studies to be carried out in GIS environments enable drought monitoring. This is vital regarding water resources management and decreasing the risks to sectors.

The present study which examines the meteorological drought of the Mediterranean Region, one of the most sensitive areas of Turkey in terms of global warming and atmospheric oscillations, by taking into account different data lengths. SPI values for SPI12, SPI6 (1), and SPI6 (2) seasons were calculated for consecutive and overlapping hydrological years (1978–1998/21 years, 1978–2008/31 years, and 1978–2018/41 years) at 28 meteorological stations. The spatial and temporal distribution of the SPI drought class, mean drought class occurrence, and MK and SS test statistics were mapped for each season and period. Spatial distribution ratios of the direction and magnitude of the trends were determined by drawing hypsometric curves. It was concluded that the extreme drought (ED) and extreme wet (EW) occurrences in the region are unstable and carry a risk compared to other subclasses in the coming years. Due to the impacts of climatic change are assessed to exhibit significant shifts from the ED to EW drought class or vice versa. The novelty of this study is the determination of spatial and temporal changes in meteorological drought propagation on consecutive and overlapping time scales. In this context, the impact of climate change on drought was monitored at overlapping and sequential time scales. This study aims to determine the spatial and temporal distribution of climate classes, drought trends, and magnitudes for the SPI12, SPI6 (1), and SPI6 (2) seasons in overlapping and consecutive hydrological

years (1978–1998/21 years, 1978–2008/31 years, and 1978–2018/41 years), and monitor the change in meteorological drought depending on the overlapping and consecutive series length of 21, 31, and 41 years.

Study area and methods

Study area and data

The Mediterranean region is considered the study area, covering 122,927 km², is one of the seven regions of Turkey and forms the southern coast of Turkey with a population of 10,584,506 in 2021. The Mediterranean Sea borders the region to the south and Syria to the northeast. The summer is hot and dry, and the winter is mild and rainy. Additionally, the province is characterized by the prevalence of the Mediterranean climate and the presence of maquis vegetation. Figure 1 shows the locations of the study area and meteorological stations used in this study. Within the aim of the study, the long-term (1978–2018) monthly precipitation series obtained from 28 meteorological observation stations which belongs to the Turkish State Meteorological Services are 2.5%, 11%, 1%, and 9% as a ratio missing observations only in Anamur, Silifke, Seydisehir, and Kozan stations, respectively. The missing observations of these stations were completed by correlation

and regression analysis as described by Landau and Everitt (2003) and Ryan et al. (2012). Meteorological stations projected coordinate system is referenced to D_WGS84_Universal Transverse Mercator (UTM)_Zone 37N to generate maps.

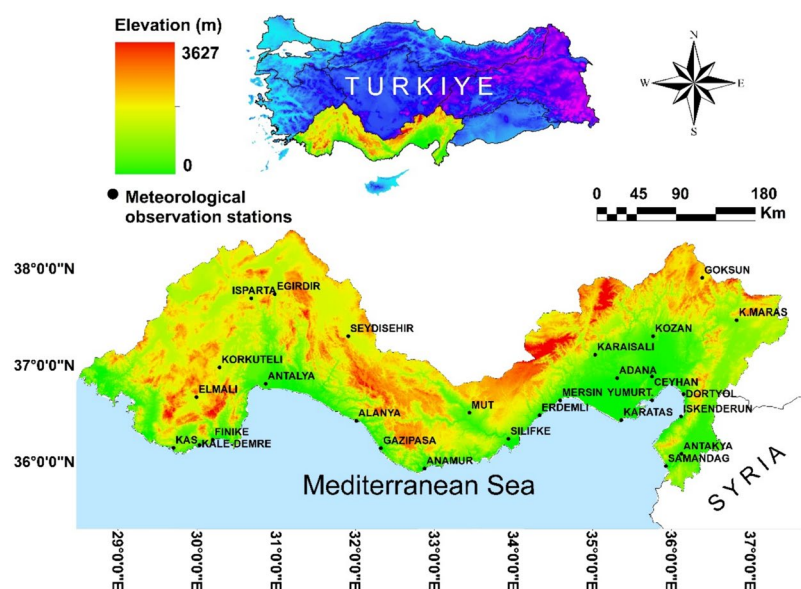
The figure shows that the elevation is higher in the northern than in the southern region. Monthly total precipitation data recorded during the hydrological years from 1978 to 2018 at 28 meteorological observation stations were used in the drought analysis of the region. In this context, SPI values for the SPI12, SPI6 (1), and SPI6 (2) seasons were calculated for consecutive and overlapping hydrological years (21, 31, and 41 years) for these stations.

Methods

Standardized precipitation index (SPI)

The standardized precipitation index (SPI) method, developed by McKee et al. (1993), is a widely preferred approach for evaluating meteorological drought (Bazrafshan et al., 2023; Kartal, 2023). *This method is advantageous over other drought indices because it only requires precipitation data to calculate the index value. Before applying the SPI method, precipitation data must be fitted to a distribution. According to Thom (1966), the gamma distribution provides a good fit for climatological*

Fig. 1 Location of the study area and spatial distribution of meteorological stations in Türkiye



precipitation time series. Angelidis et al. (2012) revealed no significant differences in SPI12 and SPI24 when the precipitation data used in the SPI method were fitted to log-normal and normal distributions instead of gamma. Topçu and Karaçor (2023) used SPI and actual precipitation index (API) drought methods to determine meteorological drought in the Aras region of Turkey. They determined that the precipitation data of six stations used in meteorological drought analysis fit the gamma distribution among Pearson type III, gamma, normal, log-normal, and exponential distributions. Based on the cumulative probability of the total quantity of precipitation recorded at each station, the SPI enables us to determine the intensity of a drought or wet spell. Using precipitation data from a single meteorological station across time, the scaling parameters and forms of the precipitation probability density function were established:

$$g(x) = \frac{1}{\beta^\alpha \Gamma(\alpha)} x^{\alpha-1} e^{-x/\beta} \quad \text{for } x > 0 \tag{1}$$

where α and β are the shape and scale parameters, respectively, x is the precipitation amount, and $\Gamma(\alpha)$ is the gamma function. The gamma function is defined as follows:

$$\Gamma(\alpha) = \int_0^\infty y^{\alpha-1} e^{-y} dy \tag{2}$$

The shape and scale parameters can be estimated using the approximation of Thom (1958):

$$\alpha = \frac{1}{4A} \left(1 + \sqrt{1 + \frac{4A}{3}} \right) \tag{3}$$

and

$$\beta = \frac{\bar{x}}{\alpha} \tag{4}$$

with

$$A = \ln(\bar{x}) - \frac{\sum \ln(x)}{n} \tag{5}$$

where \bar{x} is the mean value of the precipitation quantity; n is the precipitation measurement number; x is the quantity of the precipitation in a data sequence.

The acquired parameters are further applied to determine the cumulative probability of a certain

precipitation for a specific time period in a time-scale of all the recorded precipitation. The cumulative probability can be presented as:

$$G(x) = \int_0^x g(x) dx = \frac{1}{\beta^\alpha \Gamma(\alpha)} \int_0^x x^{\alpha-1} e^{-x/\beta} dx \tag{6}$$

Since the gamma distribution is undefined for a rainfall amount $x=0$, in order to take into account the zero values that occur in a sample set, a modified cumulative distribution function (CDF) must be considered.

$$H(x) = q + (1 - q)G(x) \tag{7}$$

With $G(x)$ the CDF and q the probability of zero precipitation, given by the ratio between the number of zeros in the rainfall series (m) and the number of observations (n).

The calculation of the SPI is presented on the basis of the following equation (McKee et al., 1993):

$$SPI = \frac{P_{ij} - P_{im}}{\sigma} \tag{8}$$

where P_{ij} =total precipitation for time scale i in year j , P_{im} =mean precipitation for time scale i , and σ_i =standard deviation of precipitation for time scale i .

The SPI value is calculated by dividing the difference between precipitation and its mean over a specified period by the standard deviation. According to the criteria of McKee et al. (1993), SPI index values are classified based on the drought classification provided in Table 1 (Balram & Fanai, 2021). Situations with a negative SPI index are termed drought, while positive values are called wet conditions. The table shows that drought and wet periods are categorized into four sub-values. The intensity of drought or wet periods increases with the magnitude of the index value.

Meteorological drought is monitored in this study using reference periods of 6 and 12 months. A new time series called October–March (SPI6 (1)), April–September (SPI6 (2)), and October–September (SPI12) is generated from the original monthly data to compute the seasonal SPI.

Serial correlation test

One of the primary challenges in trend analyses of time series data is the presence of internal dependencies, or, in other words, the existence of serial

Table 1 SPI drought classification and values (McKee et al., 1993)

Classification	SPI values
Extreme wet (EW)	2.00 or more
Severe wet (SW)	1.99 to 1.50
Moderate wet (MW)	1.49 to 1.00
Mild wet (MIW)	0.99 to 0.00
Mild drought (MID)	0.00 to -0.99
Moderate drought (MD)	-1.00 to -1.49
Severe drought (SD)	-1.50 to -1.99
Extreme drought (ED)	-2.00 or less

correlation. In the context of the Mann–Kendall trend test, data with a positive serial correlation leads to the rejection of the null hypothesis of no trend in the trend analysis results (Wang et al., 2020). Therefore, if autocorrelation exists among consecutive data points, a trend analysis should not be applied; instead, “pre-whitening” should be employed to remove serial autocorrelation. The trend analysis should then be applied to the resulting new series (Shifteh Some’e et al., 2012). In engineering, the lagged autocorrelation coefficient for delayed internal dependencies can be calculated using Eq. 9 (Mohsin & Gough, 2009).

$$r_1 = \frac{\sum_{i=1}^{n-1} (x_i - \bar{x})(x_{i+1} - \bar{x})}{\sum_{i=1}^n (x_i - \bar{x})^2} \quad (9)$$

where x_i and x_{i+1} represent the i .th and $i + 1$.th observation values, respectively; \bar{x} denotes the mean of the observation series, and n represents the number of observations in the series. The calculated $CL(r_i)$ value in the study is deemed to indicate that autocorrelation between consecutive observations is insignificant at a

5% significance level if it falls within the lower and upper confidence limits calculated with Eq. 10, with a 95% probability (Gocic & Trajkovic, 2013).

$$\frac{-1 - 1.96\sqrt{n-2}}{n-1} \leq CL(r_1) \leq \frac{-1 + 1.96\sqrt{n-2}}{n-1} \quad (10)$$

Mann–Kendall (MK) test

The Mann–Kendall (MK) test is a recommended test by the World Meteorological Organization and is widely used to detect trends in time series data. In the MK test statistic calculations, denoted as S in Eq. 11, n represents the number of data points, and x_j and x_k , with $j > k$, represent the annual values for years j and k , respectively. The sign of $(x_j - x_k)$ in Eq. 12 can be defined accordingly (Gumus et al., 2023; Lin et al., 2020; Yilmaz et al., 2020).

$$S = \sum_{k=1}^{n-1} \sum_{j=k+1}^n \text{sgn}(x_j - x_k) \quad (11)$$

$$\text{sgn}(x_j - x_k) = \begin{cases} +1 & \text{if } x_j - x_k > 0 \\ 0 & \text{if } x_j - x_k = 0 \\ -1 & \text{if } x_j - x_k < 0 \end{cases} \quad (12)$$

The value of S expressed in Eq. 6 approximately follows a normal distribution with mean ($E[S]$) and variance ($Var(S)$) when $n \geq 10$, and the Z test is used. In $Var(S)$ calculations, q represents the number of grouped data in the dataset, and t_p denotes the number of data points in the p -th group. The Mann–Kendall trend test Z statistic, defined by Eq. 14, can be calculated using S and $Var(S)$ given in Eq. 13 (Keskiner & Cetin, 2023; Yue & Wang, 2002).

$$E[S] = 0, \text{Var}(S) = \frac{1}{18} \left[n(n-1)(2n+5) - \sum_{p=1}^q t_p(t_p-1)(2t_p+5) \right] \quad (13)$$

$$Z = \begin{cases} \frac{S-1}{\sqrt{Var(S)}} & \text{if } S > 0 \\ 0 & \text{if } S = 0 \\ \frac{S+1}{\sqrt{Var(S)}} & \text{if } S < 0 \end{cases} \quad (14)$$

The presence of a trend is determined using the Z statistic. The MK test statistic ($Z_{MK\text{test}}$) is checked

against Z values from the standard typical distribution table. If $-Z_{1-\alpha/2} \leq Z_{MK\text{test}} \leq Z_{1-\alpha/2}$, the null hypothesis stating no trend is accepted. A positive Z value indicates an increase in the variable under investigation, while a negative Z value signifies a decrease in the series. In this study, the obtained $Z_{MK\text{test}}$, calculated based on the results, is evaluated within the confidence

interval of $Z_{table} = \pm 1.96$ obtained from the typical distribution table at a 5% significance level.

Sen’s slope method

The Mann–Kendall trend test does not provide information about the trend’s magnitude or direction in the studied data (Lettenmaier et al., 1994). However, the non-parametric Sen’s slope method uses a linear model to provide information about the amount and direction of the trend in time series data (Gümüř et al., 2023; Salmi et al., 2002). In Eq. 15, n represents the number of data points, and N represents the number of Sen’s slope estimates that need to be calculated in the time series for observed data at times j and k (x_j and x_k) (Kaur et al., 2021). The Sen’s slope trend statistic (Q_i) for N pairs of observations is calculated with Eq. 16, and the obtained Q_i values are arranged in ascending order to find the median value. Depending on whether the number of N is odd or even, the median of Q_i values (Q_{median}) is obtained as expressed in the equation set shown in Eq. 17. The Q_{median} value represents the unit-time change in the relevant observations. When the Q_{median} value is positive, it is decided that there is an increasing trend; if it is negative, a decreasing trend is concluded. The statistical significance of the Q_{median} value is tested at a 5% significance level to complete the analysis (Sen, 1968).

$$N = \frac{n(n - 1)}{2} \tag{15}$$

$$Q_i = \frac{X_j - X_k}{j - k}, j > k \text{ and } i = 1, 2, 3, \dots, N \tag{16}$$

$$Q_{medyan} = \begin{cases} \frac{Q_{(n+1)}}{2} & , \text{ if } N \text{ is odd number} \\ \frac{\left| \frac{Q_{(N)}}{2} + \frac{Q_{(N+2)}}{2} \right|}{2} & , \text{ if } N \text{ is even number} \end{cases} \tag{17}$$

Inverse distance-weighted interpolation technique (IDW)

The inverse distance-weighted interpolation (estimation) technique can be employed to estimate the potential value at an unobserved point by utilizing data from n observed points within an area. The estimated value, \hat{g} , is determined by assigning weights to

the observations surrounding the point to be evaluated, as illustrated in Eq. 18 (Liu et al., 2021).

$$\left. \begin{aligned} d_{i0} &= \sqrt{(x_0 - x_i)^2 + (y_0 - y_i)^2} \\ w_i &= \frac{d_{i0}^{-p}}{\sum_{i=1}^n d_{i0}^{-p}}, \sum_{i=1}^n w_i = 1, \hat{g} = \sum_{i=1}^n w_i g_i \end{aligned} \right\} \tag{18}$$

where n represents the number of observations used in the calculation (prediction); d_{i0} is the Euclidean distance (m) between the observed and predicted points (meters); (x_0, y_0) denotes the UTM coordinates (m) of the expected point (meters); (x_i, y_i) represents the coordinates of the observed point (meters); w_i is the weight assigned to the observation value g_i ; p is the exponent value that ensures a decrease in weights assigned to more distant points; \hat{g} is the estimated value at the predicted point; and g_i represents the observed value.

Change in the occurrence percentages of drought classes in different data record lengths

Equation 19 was used to calculate the percentage change (PC) in the occurrence percentage of different drought classes, as shown in Table 1 for drought indices values at different data record lengths.

$$PC = \left(\frac{X_{i+1} - X_i}{X_i} \right) \times 100 \tag{19}$$

X_i and X_{i+1} represent the occurrence ratios in the short and long data record lengths, respectively.

Graphical analysis of the hypsometric curves of the MK and Sen’s slope statistics

The hypsometric curves of MK and Sen’s slope statistics depict the distribution of the MK trend and Sen’s slope trend magnitudes, as in the height-area distribution (Chow et al. 1988). Hypsometric curves can be adapted for parameters such as the areal distribution of surface runoff and drought indices (Keskiner et al., 2020; Vivoni et al., 2008). In this study, maps of MK (Z) and Sen’s slope (Q) statistics for consecutive and overlapping 21-, 31-, and 41-year SPI time series in the SPI12, SPI6 (1), and SPI6 (2) seasons were generated at a resolution of 200 m × 200 m in raster format. In developing the hypsometric curves, the Z and Q statistics values and the areas covered by these statistics in the pixels representing the basin were utilized.

Results

Descriptive statistics

Using the monthly total precipitation values observed during the hydrological years 1978–2018 from 28 meteorological observation stations in the Mediterranean basin, the long-term averages of the annual total precipitation values (P) for each station were calculated. Precipitation series representing long-term averages were divided into 21-year (1978–1998), 31-year (1978–2008), and 41-year (1978–2018) series in a consecutive and overlapping manner. Descriptive statistics of these series were determined, and it was observed that central tendency and variability did not create significant differences in consecutive and overlapping long-term averages. Detailed descriptive statistics derived from these series are presented in Table 2. Examining the table values reveals a lack of significant differences in central tendency and variability between consecutive and overlapping long-term averages. This observation can be attributed to calculating descriptive statistics grounded in the averages of long-term rainfall series. The approximation of rainfall variability across different series lengths, namely, 21, 31, and 41 years ($C_v=27, 27, \text{ and } 26$), consistently supports this finding.

A mapping exercise was undertaken for annual average rainfall to delve into spatial and temporal variations in variability. This mapping considered the averages representing each meteorological station, as illustrated in Fig. 2. Based on consecutive and overlapping series averages, spatial distribution maps yielded the insightful conclusion that there is no significant alteration in long-term rainfall averages within the Mediterranean region. A thorough examination of the 21-, 31-, and 41-year time scales applied in the study area revealed that the Mut and Korkuteli stations experienced the lowest average rainfall (360–460 mm), while the highest average rainfall (1060–1160 mm) was observed in the

Alanya, Antalya, and Antakya stations. When scrutinizing the locations of these stations, a noteworthy pattern emerged, indicating that the central and northwestern parts of the study area receive comparatively less precipitation than other regions.

Results of the independence test

Within the scope of the research, 6 and 12-month SPI (standardized precipitation index) values were calculated for 21, 31, and 41 consecutive and overlapping hydrological years. Stations exhibiting internal dependence in SPI12, SPI6 (1), and SPI6 (2) seasons were determined, and the internal dependence control for all stations considered in the study is presented in Fig. 3. As seen in the figure, it is noteworthy that the upper and lower confidence limits of the autocorrelation drawn with the horizontal dotted red line narrow as the series length increases (from 21 to 41 years). As the SPI seasons changed from SPI12 to SPI6 (1) and SPI6 (2) months, the number of stations showing internal dependence tends to decrease, respectively. In 12-month SPI values, Isparta, Eğirdir, Elmalı, Finike, and Kale-Demre stations exhibit internal dependence at three different time scales. Before applying MK trend analysis to the stations showing internal dependence, a “pre-whitening” technique was applied to remove autocorrelation from each period and from the overlapping 21-, 31-, and 41-year series.

Drought analysis with the SPI method

The average percentage of SPI drought class occurrence

Within the scope of this study, consecutive and overlapping SPI (standardized precipitation index) series were created for 21, 31, and 41 years during the SPI12,

Table 2 Descriptive statistics of overlapping and successive sequential 21-, 31-, and 41-year precipitation (P) time series

P (mm)	Mean	Stand. dev	Median	Min	Max	Skewness	Kurtosis	Coef. of variation (%)
P_21	758.7	203.1	771.3	364.8	1162.0	-0.08	-0.17	27
P_31	754.0	200.0	773.1	362.5	1102.0	-0.12	-0.42	27
P_41	759.5	198.3	787.0	370.2	1129.5	-0.14	-0.39	26

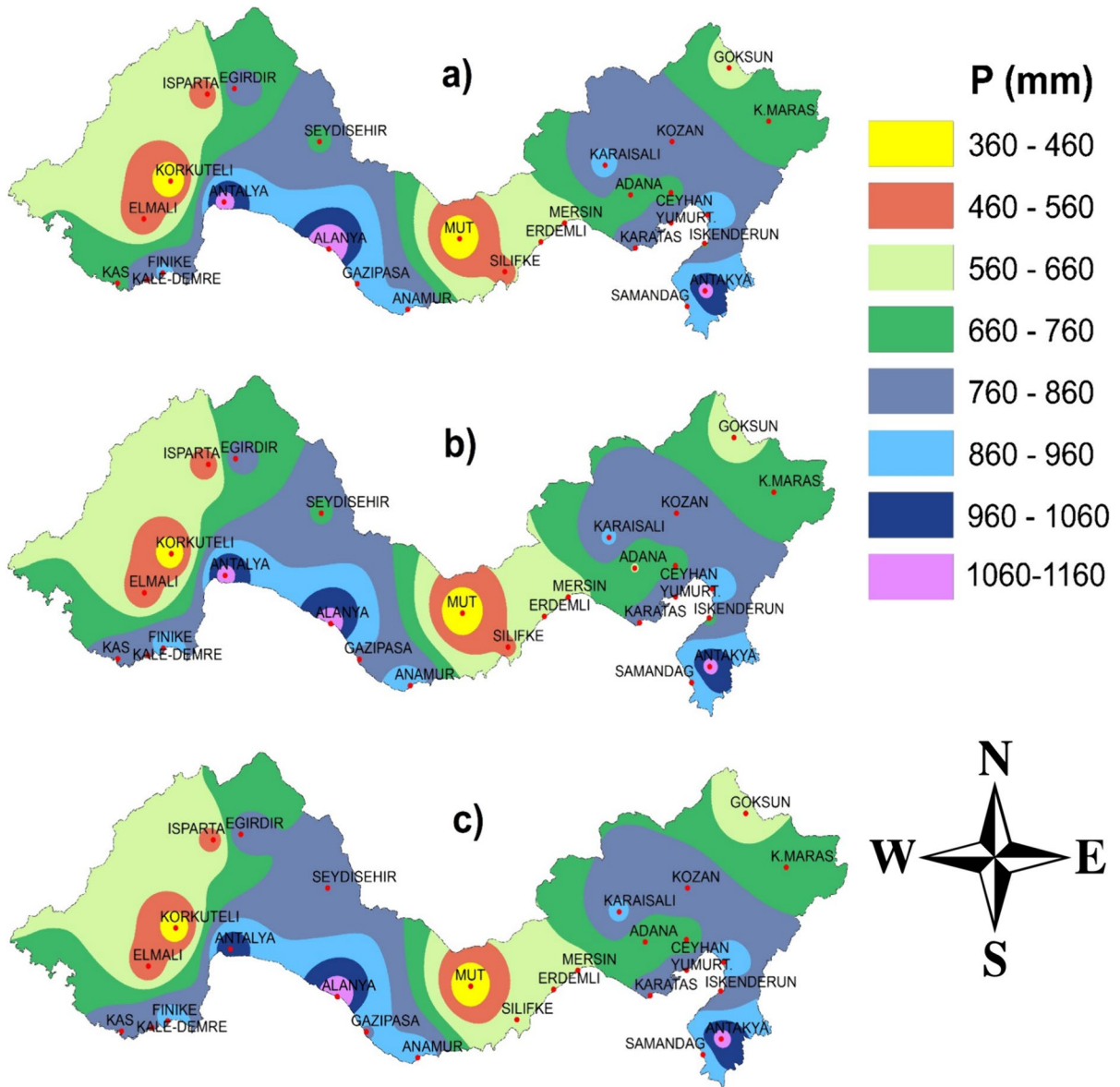


Fig. 2 Average annual precipitation of meteorological stations overlapping and successive sequential **a** 21-, **b** 31-, and **c** 41-year periods

SPI6 (1), and SPI6 (2) seasons using monthly total precipitation values recorded over 41 years (1978–2018). The formation percentages of these series according to the SPI index classification given in Table 1 are illustrated in Fig. 4. Upon examining the figure, it is noteworthy that there is an inverse correlation between the EW-ED, SW-SD, MW-MD, and MIW-MID drought classes in the 21-, 31-, and 41-year series during the SPI12, SPI6 (1), and SPI6 (2) seasons.

The changes (%) in drought classes (PC) between consecutive and overlapping 21–31 (10 years), 31–41 (10 years), and 21–41 (20 years) yearly series in SPI time scales are provided in Table 3. As the table shows, during the SPI6 (1) season, the changes in drought (D) occurrences in SPI values continuously decreased (−4.8, −3.2, −7.8). However, during the SPI12 and SPI6 (2) seasons, the changes in drought occurrences at 21–31, 31–41, and 21–41 time scales

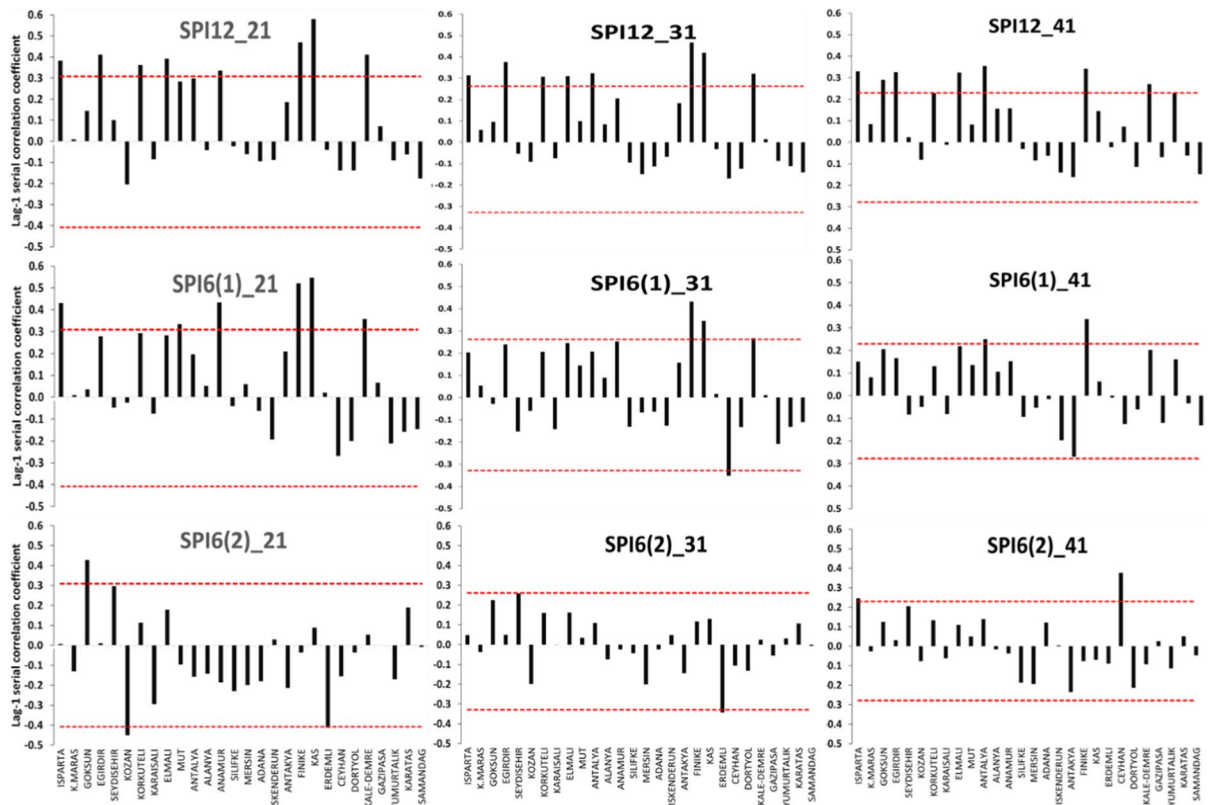


Fig. 3 Lag-1 serial correlation coefficient of the SPI series at the different seasonal scales

occurred in the sequence of increase–decrease–increase, respectively (7.1, −4.1, 2.6; 4.5, −2.5, 1.9).

The most noteworthy aspect of the changes in SPI drought classes at the 21–31, 31–41, and 21–41 time scales is the consistency in the increase and decrease in the formation of drought classes during SPI seasons. For example, during the SPI6 (2) season, there is a continuous increasing trend in SD formation (35.5, 4.8, 41.9), while MD and ED formations in the same season consistently decreased (−10.9, −5.1, −15.5; −12.1, −3.4, −15.2). The increase in SD while MD and ED always decrease suggests a stabilization trend toward the SD class during this period. In the SPI12 season, a decreasing trend in MW formation (−2.8, −2.9, −6.0) was identified. In the SPI6 (1) season, an increase in the MIW class and a continuous decrease in the MID class were observed (11.2, 3.9, 15.5; −6.2, −4.3, −10.3). When considering the variability of drought classes in the Mediterranean region for each period of drought and wet classes, the absolute variability of the EW, SW, ED, and SD

drought classes is represented as 328.3, 139.8, 309.0, and 191.8, respectively. The absolute variability of the MW, MIW, MID, and MD drought classes is determined to be 61.8, 58.8, 60.8, and 65.3, respectively. These results indicate that the region's extreme moisture and drought classes do not exhibit absolute stability compared to other subclasses, suggesting a dynamic nature and posing a risk factor. In the study area, climatic change impacts are assessed to exhibit significant shifts (Handmer et al., 2012) from the ED to EW drought class or vice versa in 10-year time intervals.

Spatiotemporal changes in drought classes

SPI series calculated using data of three different record lengths for the SPI12, SPI6 (1), and SPI6 (2) seasons for each station were considered, and the median values of these SPI series were used to create maps of drought classes for the study area, as presented in Fig. 5. The most striking observation in the

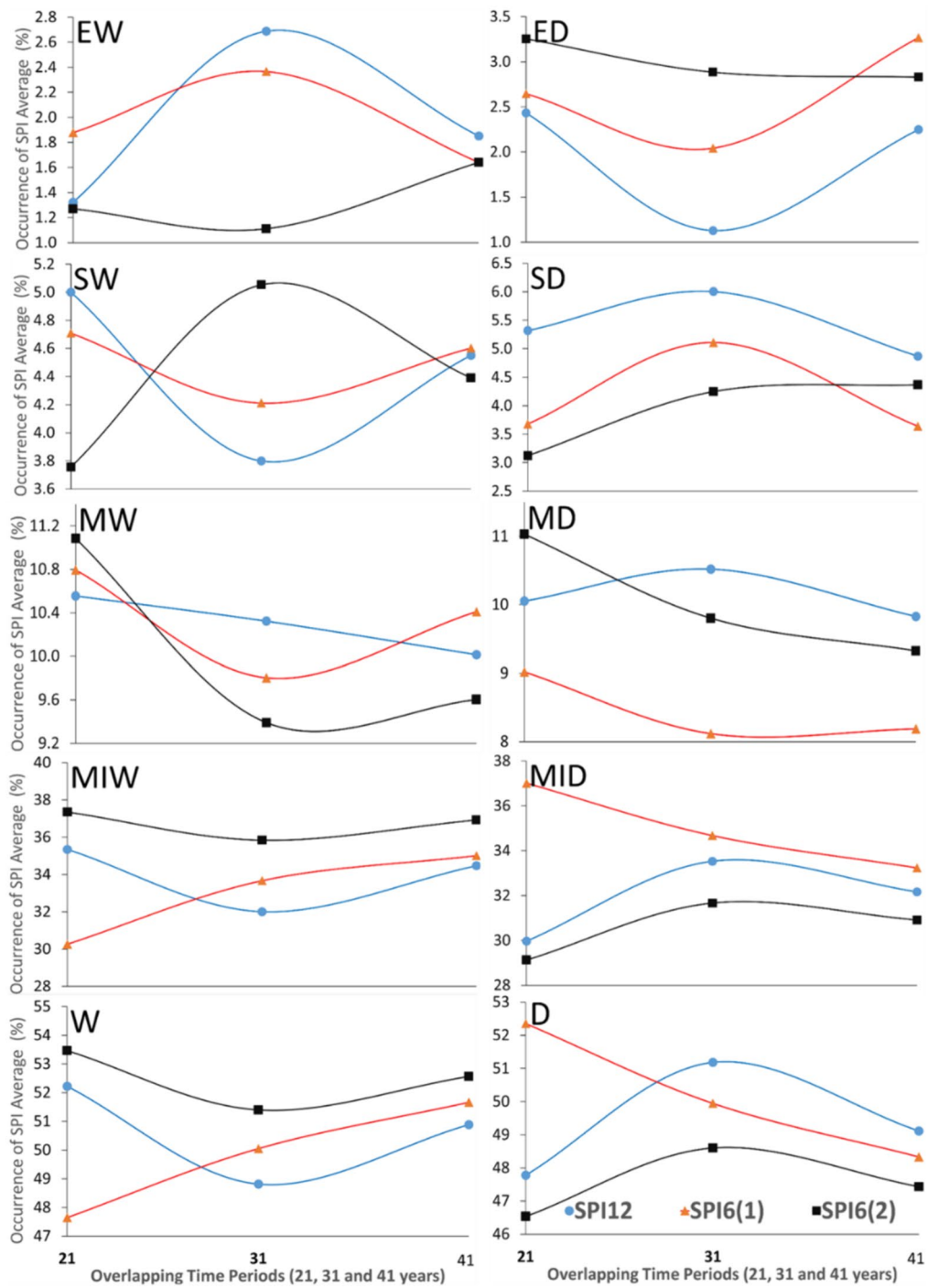


Fig. 4 The average of SPI drought class overlapping periods (1978–1998, 1978–2008, and 1978–2018)

Table 3 Pairwise comparison (%) of changing drought class occurrence (PC) overlapping periods (21 and 31, 31 and 41 and 21 and 41 years)

SPI Seasonal	SPI12			SPI6 (1)			SPI6 (2)		
	Changing in 31	Changing in 41	Changing in 41	Changing in 31	Changing in 41	Changing in 41	Changing in 31	Changing in 41	Changing in 41
Increase (%)	According to 21	According to 31	According to 21	According to 21	According to 31	According to 21	According to 21	According to 31	According to 21
Decrease (%)	According to 21	According to 31	According to 21	According to 21	According to 31	According to 21	According to 21	According to 31	According to 21
EW	107.7	-29.6	31.6	26.3	-33.3	-15.8	-15.4	45.5	23.1
SW	-24.0	21.1	-8.7	-10.6	9.5	-2.1	34.2	-13.7	15.8
MW	-2.8*	-2.9*	-6.0*	-9.3	6.1	-3.7	-15.3	2.1	-13.5
MIW	-9.3	7.8	-2.3	11.2**	3.9**	15.5**	-4.3	3.1	-1.3
MID	11.7	-3.9	6.8	-6.2*	-4.3*	-10.3*	8.9	-2.5	6.2
MD	4.0	-6.7	-3.1	-10.0	1.2	-8.9	-10.9*	-5.1*	-15.5*
SD	13.2	-18.3	-8.2	37.8	-29.4	-2.7	35.5**	4.8**	41.9**
ED	-54.2	100.0	-9.1	-23.1	65.0	26.9	-12.1*	-3.4*	-15.2*
W	-6.5	4.3	-2.6	5.3**	3.2**	8.6**	-3.9	2.3	-1.7
D	7.1	-4.1	2.6	-4.8*	-3.2*	-7.8*	4.5	-2.5	1.9

The yellow and blue backgrounds represent increases and decreases for successive overlapping time scales, respectively

*Continuous decrease over successive overlapping time scales

**Continuous increase over successive overlapping time scales

maps is that the study area is represented only by the MIW and MID drought classes. As seen in Fig. 4, MIW and MID drought class formation percentages in the SPI12, SPI6 (1), and SPI6 (2) seasons at 21-, 31-, and 41-time scales are represented with the highest values. Therefore, the median values of the series, representing the central tendency, are represented by MIW and MID drought class values. These have suppressed and non-represent other drought classes in the spatial distribution.

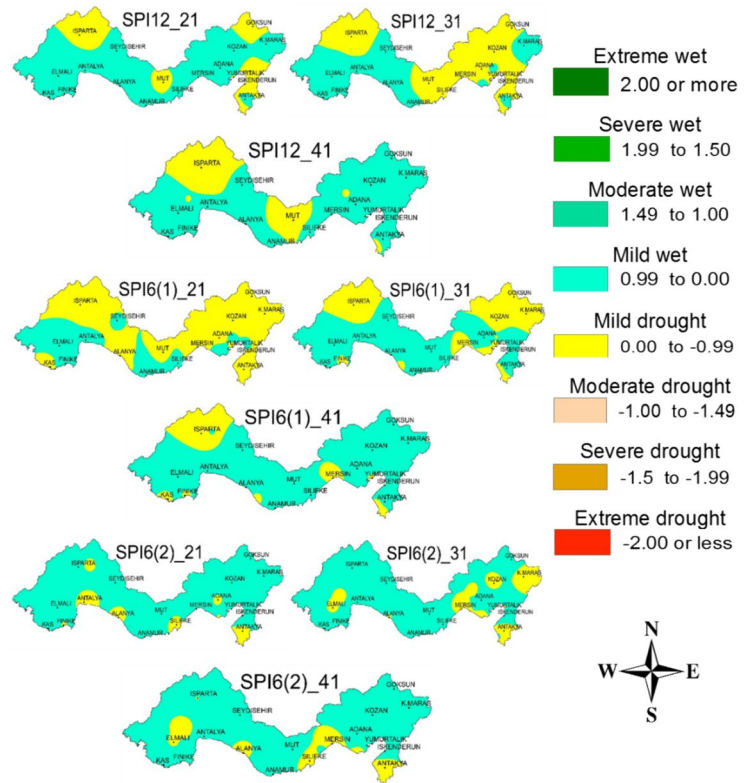
Upon examining the maps, during the SPI12 season at the 21–31 year time scale, the MID drought class spread eastwards, encompassing Mut, Silifke, Mersin, Adana, and Kozan regions. However, on the 31–41 year time scale, this spread halted, and the MIW drought class regained dominance over the region. In the 21–41 year time scale, while MIW dominates spatially, it is observed that the MID class in the Mut and Isparta regions stabilizes, similar to the other periods. In the SPI6 (1) season, it can be said that the MID class loses its dominance in the region at the 21–31, 31–41, and 21–41 year time scales, giving way to the MIW drought class. However, the Isparta region maintains a stable MID drought class across all time scales, as observed in the SPI12 season. In the SPI6 (2) season, it was determined that the MIW drought class exhibited a stable characteristic across all time scales, establishing dominance over the Mediterranean region.

Due to the nonrepresentation of other drought classes in the maps (Fig. 5), which were generated based on the median values of the SPI series, the spatial distributions of the formation percentages of

drought classes given in Table 1 for each SPI period and 21-, 31-, and 41-time scales are presented in Figs. 6, 7, and 8, respectively. From Fig. 6, for the SPI12 season at the 21-year time scale, the spatial distribution of EW covers the southeastern, central, and northeastern parts of the region, exhibiting a dominant appearance with a percentage of 0–2. This situation changed at the 31-year time scale, and the EW class occurrence percentage increased to 2–4, covering the entire region. However, over the past 41 years, the occurrence rate of the EW drought class has again decreased to 0–2 in the eastern and western parts of the region, while a stabilization trend of 2–4 is observed in the northeastern and central parts. Considering the spatial distribution of the ED drought class, in the 21-year time scale, there was an occurrence of 4–5 in the central part of the region. In the 31 time scale, especially in the central region, there were sharp decreases in the occurrences of the ED drought class, which can be considered significant (1–2%). When considering the 41-year scale, the region's overall occurrence of the ED drought class has increased toward 2–4.

When examining the spatial distribution of the SW drought class given in Fig. 6, weighted occurrence rates were approximately 0–8% for consecutive 21-, 31-, and 41-year time scales, and no significant differences were observed. An increasing trend in SW drought class expansion was identified consecutively at the 21-, 31-, and 41-year scales. While observing the distribution of the SD drought class in the Mediterranean region, consecutive decreases were observed at the 21-, 31-, and 41-year time scales, and

Fig. 5 The median-based drought classification at the different seasonal scales of the SPI method

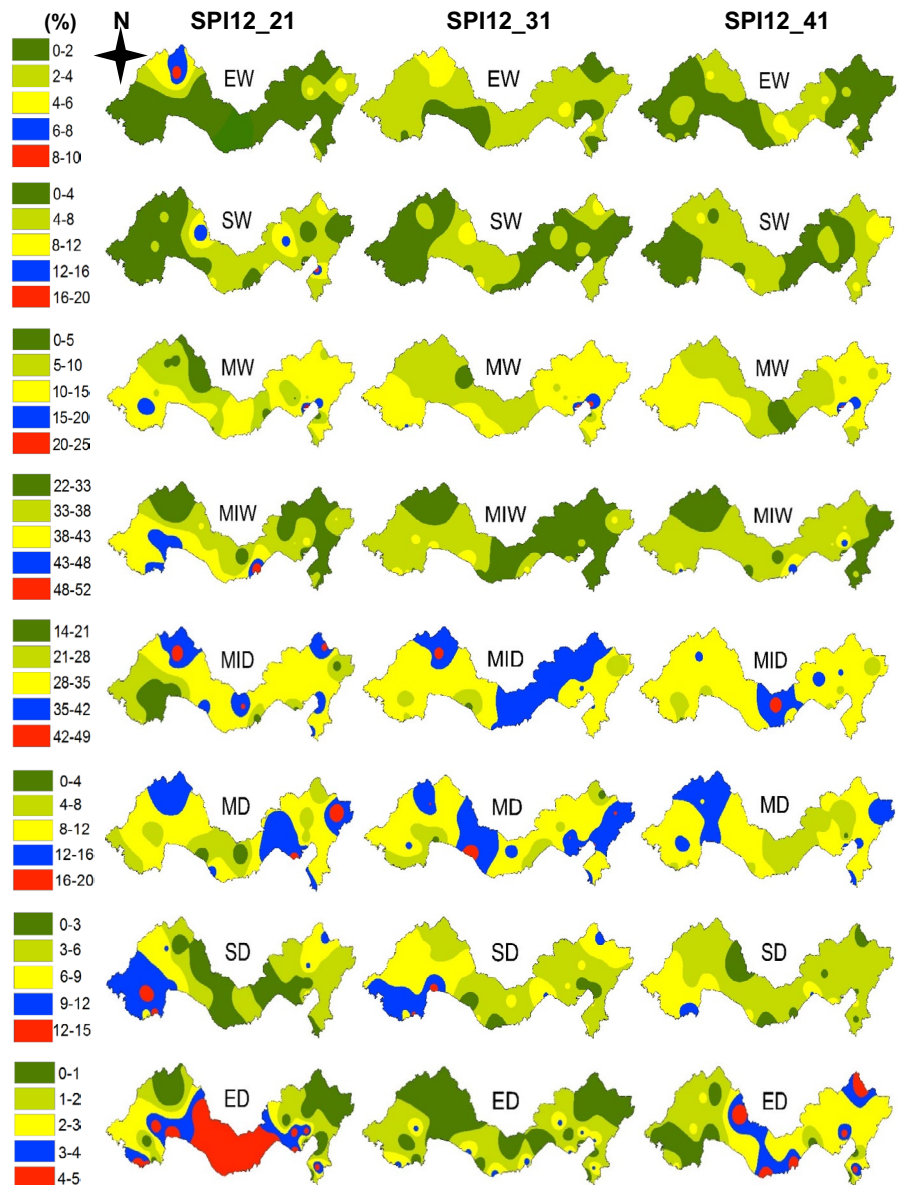


a stabilization trend in SD drought class occurrences was determined at the regional level, ranging between 3 and 6%. MW drought class occurrences predominantly occurred in the region at 0–15% levels for all time scales. The MD drought class occurred predominantly at levels of 4–16% in the area for 21- and 31-year time scales, while for the 41-year time scale, weighted MD drought class occurrences were determined to shift toward 4–12%. While the spatial spread of the MIW drought class in the region showed a significant decrease at the 21- and 31-year time scales, consecutive stabilization trends were identified at a range of 33–38% across the region for the 21-, 31-, and 41-year time scales. The weighted occurrence rate of the MID drought class in the 21-year time scale was 21–35%. Considering the last 10 years with the 31-year time scale, it was determined that the weighted occurrence increased to the level of 28–41%. In the 41-year time scale, a stabilization trend in forming the MID drought class was observed in the 28–35% range. In the SPI12 season at the 21-, 31-, and 41-year scales, consecutive decreases in extreme moisture and drought formations, such as

EW, SW, ED, and SD drought classes, were identified across the region. However, as seen in Table 1, it is noteworthy that there is significant variability in formations in binary comparisons. In the subclasses of drought and moisture, it was observed that the formations of drought classes consecutively stabilized across all time scales.

As observed in Fig. 7, for the SPI6 (1) season, the weighted occurrence rate of the EW drought class at the 21-year scale is predominantly approximately 0–3%. Over the past 10 years, this dominant occurrence at the 0–3% level has shown an expanding trend as we transition to the 31-year time scale. In the 41-year time scale, it is determined that this occurrence (0–3%) has spread across the region, indicating a stabilization trend. At the 21-year scale, the ED drought class formed in the central part of the region at a rate of 4–5%, while in the east and west of the region, this rate changed to 0–3%. In the 31-year time scale, the formation of the ED drought class occurred at 0–3% across the entire region, and compared to the 21-year time scale, the formation of the ED drought class in the region decreased. In the 41-year time

Fig. 6 The map of average drought class occurrence (%) of SPI12 season



scale, while the formation of the ED drought class locally increased to 5–7% in the eastern region, there has been an increase in ED drought class formations across the province over the past 10 years.

From the spatial pattern of the SW drought class given in Fig. 8, occurrences across the entire region at the 21-year scale are in the range of 0–15%, while at the 31-year scale, occurrences have decreased to the range of 0–12%. At the 41-year scale, SW drought class formations occurred at a rate of 0–9%, tending to stabilize at approximately 3–4%. For the SD drought class in the Mediterranean region, formations

at the 21-year scale ranged from 0–10%, with a predominant occurrence of SD drought class formations at 3–7% in terms of spatial distribution. Over the past 10 years, in the 31 years, occurrences in the region continued at a rate of 0–10%. However, the SD drought class occurrence at 7–10% in the central and western parts of the region has increased over the past decade, indicating an increase in SD drought class formations. In the 41-year time scale, with occurrences ranging from 0 to 7%, the spatial distribution of SD drought class formations indicated a tendency toward stabilization. The MW drought

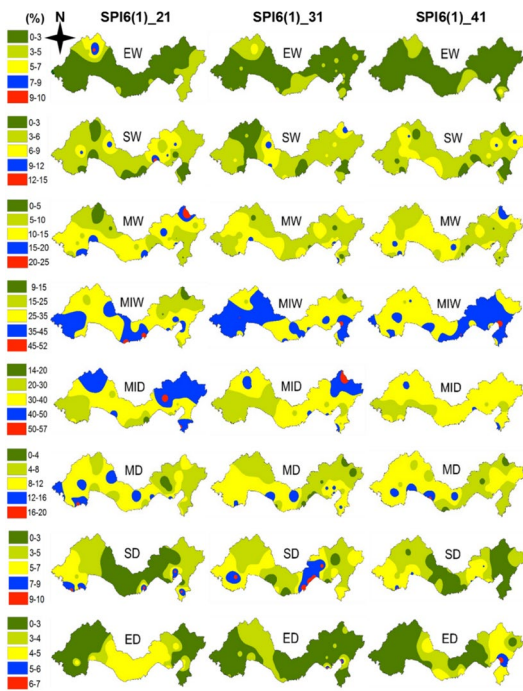


Fig. 7 The map of average drought class occurrence (%) of SPI6 (1) season

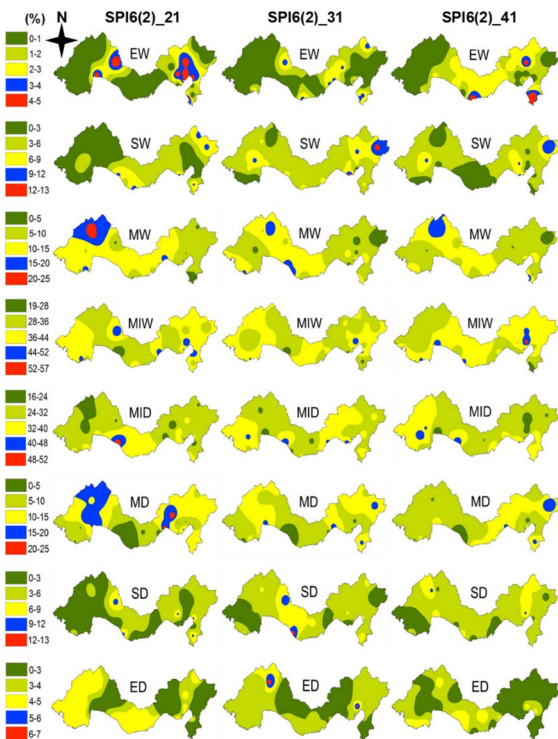


Fig. 8 The map of average drought class occurrence (%) of SPI6 (2) season

class formations did not show significant differences at the 21-, 31-, and 41-year scales. The predominant occurrence rate of the MW drought class at all scales varied between 5 and 15%. The spatial distribution of MD drought class formations exhibited a similar character to the MW drought class, with the predominant occurrence rate in the region ranging from 4 to 12% across all scales. For the MIW class, the predominant occurrence rate in the spatial distribution across all scales was approximately 25–45%, but a tendency toward stabilization was observed at the 41-year time scale. In the 21-year time scale, the predominant occurrence rate for the MID drought class ranged from 30 to 50%, but after 10 years, this rate decreased to approximately 20–40%. In the 41-year time scale, the occurrence rate of the MID drought class in the region showed a tendency toward stabilization at approximately 30–40%. In the SPI6 (1) period, considering all drought classes and time scales, it has been determined that the different levels of formations in the 21-year series decreased in the 31-year time scale and further decreased in the 41-year scale, indicating a tendency for each drought class to stabilize.

For the SPI6 (2) season, when examining the figures given in Fig. 8, it can be observed that the spatial distribution of the EW drought class in the 21-year time scale is predominantly in the eastern and central regions of the region, with an occurrence rate of 0–1%. However, in the region’s western part, EW drought class formations at a 3–5% rate are notable. In the 31-year time scale, EW formations representing 1–3% of the region have been observed, indicating a trend toward stabilization. This trend has increased toward a 3% occurrence rate over the past 10 years. In the 21-year time scale, the predominant occurrence of the ED drought class in the eastern and central parts of the region was 4–5%, while in other areas, it was 0–3%. At the 31- and 41-year scales, the predominant formation of the ED drought class decreased by 3–4% and 0–3%, respectively. When examining the spatial distribution of the SW drought class, formations at the 21-year scale were observed to be approximately 0–9% throughout the region. At the 31-year scale, the formations were stable in the 3–6% range. In the 41-year time scale, while the SW formations occurred at a rate of 0–9% throughout the region, considering the 21–31 and

41-year scales, a stabilization trend toward 3–6% was observed. For the SD drought class in the Mediterranean region, formations in the 21-year scale were observed in the range of 0–6%, and over the past 10 years, the weighted occurrence in the 31-year time scale tended to stabilize at 3–6%. This trend continued in the 41-year time scale throughout the region. MW drought class formations at the 21-year scale were observed predominantly in the east of the province, around Isparta and Eğirdir, except for occurrences in the 15–25% range. No significant differences in occurrences were observed at the 21–31 and 41-year scales. It was determined that the MW drought class stabilized in the region at a rate of 5–15%. The spatial distribution of the MD drought class showed a pattern similar to that of the MW drought class. While occurrences in the 21-year time scale extended to areas around Isparta, Eğirdir, and Antalya at a rate of 15–25%, in the 31- and 41-year time scales, the predominant occurrence rate of the MD drought class in the region varied in the range of 5–15%. For the MIW drought class, it was observed that there was stabilization in spatial distribution throughout the area at an occurrence rate of 28–44% for all time scales. The predominant occurrence rates for the MID drought class were 24–40% for all time scales, with differences only in spatial distributions.

During the SPI6 (2) period, when all drought classes and 21-, 31-, and 41-time scales are considered together, a consecutive decrease in EW, SW, ED, and SD drought class formations was observed throughout the region. However, it is important to note that there is significant variability in formations, as indicated by the dual comparisons in Table 1. In the subcategories of drought and wetness, it was found that each drought class tends to stabilize consecutively, similar to the pattern observed during the SPI6 (1) season.

Results of the trend test

Within the scope of this research, the MK and Sen's slope tests were applied to consecutive and overlapping 21-, 31-, and 41-year SPI time series for the SPI12, SPI6 (1), and SPI6 (2) periods. MK (Z) and Sen's slope (Q) trends and trend magnitudes were obtained for each station for different periods and

consecutive time scales. Mann–Kendall trend maps and Sen's slope trend maps for each distinct SPI period and consecutive overlapping time scales were obtained through the IDW method using the Z and Q statistics representing each station.

Mann–Kendall trend maps

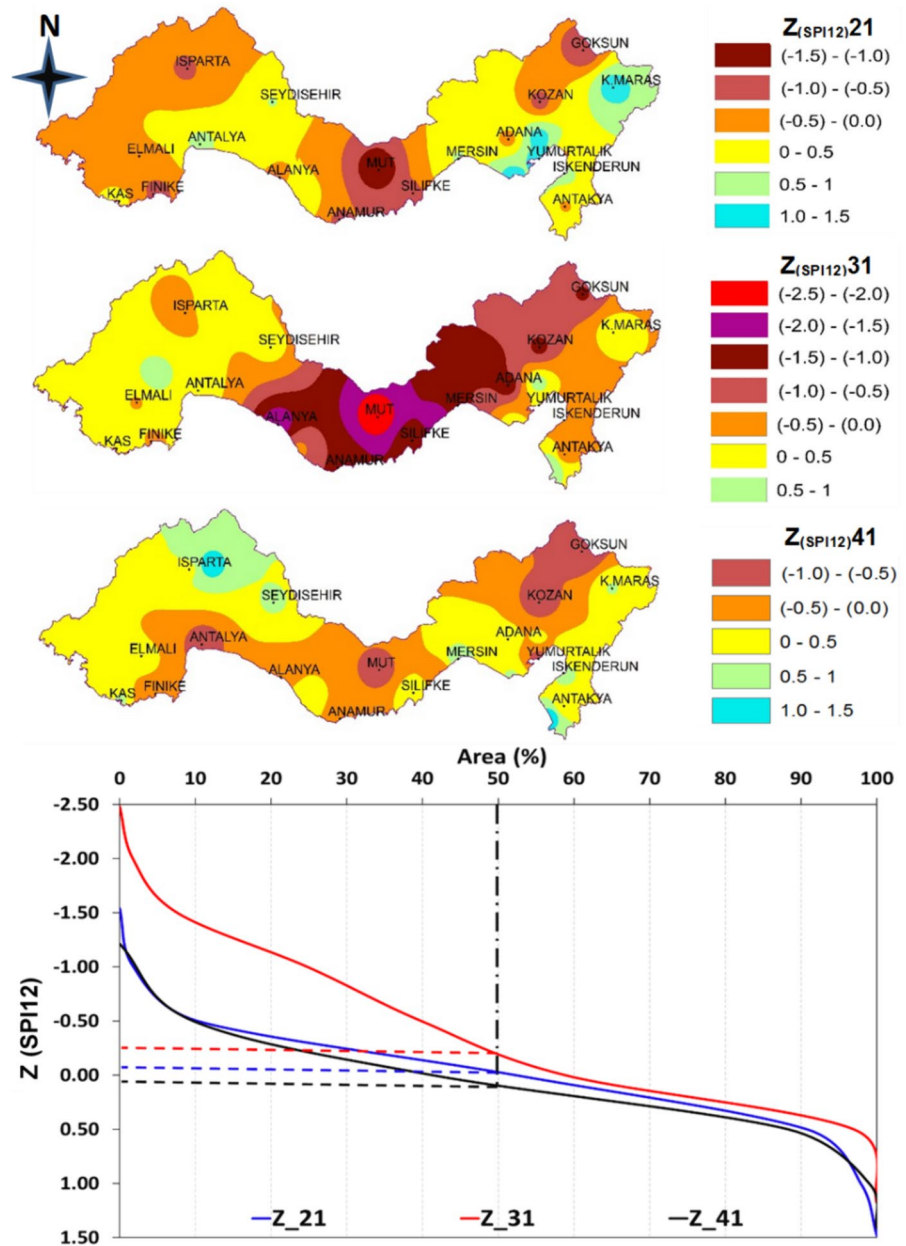
The MK statistics representing each station for the SPI12, SPI6 (1), and SPI6 (2) seasons at 21-, 31-, and 41-year time scales were utilized to obtain the spatial distributions of the MK statistics and the hypsometric curves of the MK statistics. The spatial and temporal distribution of MK statistics in the Mediterranean region for all time scales of SPI12 is illustrated in Fig. 9. The Mann–Kendall trend maps and median-based drought class maps shown in Fig. 5 were jointly considered in determining drought's spatial and temporal spread.

When examining the spatial distribution of the $Z_{(SPI12)21}$ statistic at the 21-year time scale ($Z_{(SPI12)21}$) for the SPI12 period, it is considered that the decreasing trends occurring in the east of the region, particularly in the middle region around Mut, with Z values between -1.5 and -1.0 , need to be taken into account. Over the past 10 years, significant trends have occurred at the 31-year time scale in the region. Significant decreasing trends have been observed, especially in the middle area around Mut, and decreasing trends continue toward the region's east.

Considering the 41-year time scale, although there are no significant trends in the overall region in both increasing and decreasing directions, it has been determined that reducing trends, especially around Mut in the east of the area, persist, as observed in the 21-year time scale. For the SPI12 period, when considering the Z statistic according to hypsometric curves for 50% of the region, it is determined that at the 21-year time scale, Z is ≤ -0.01 , over the past 10 years Z is ≤ -0.03 , and at the 41-year time scale, Z is ≤ 0.01 . Regarding the trends in time scales based on the spatial average in the region, statistically nonsignificant decreasing-decreasing and increasing trends have occurred.

Considering the 21, 31 and 41-year time scales of the SPI12 season only significant decreasing trends ($Z \leq -1.96$) were observed in the 31-year time scale. It was determined that the drought trend increased in the vicinity of Mut. According to the climate class

Fig. 9 The MK trend maps and hypsometric curves of SPI12 at different time scales

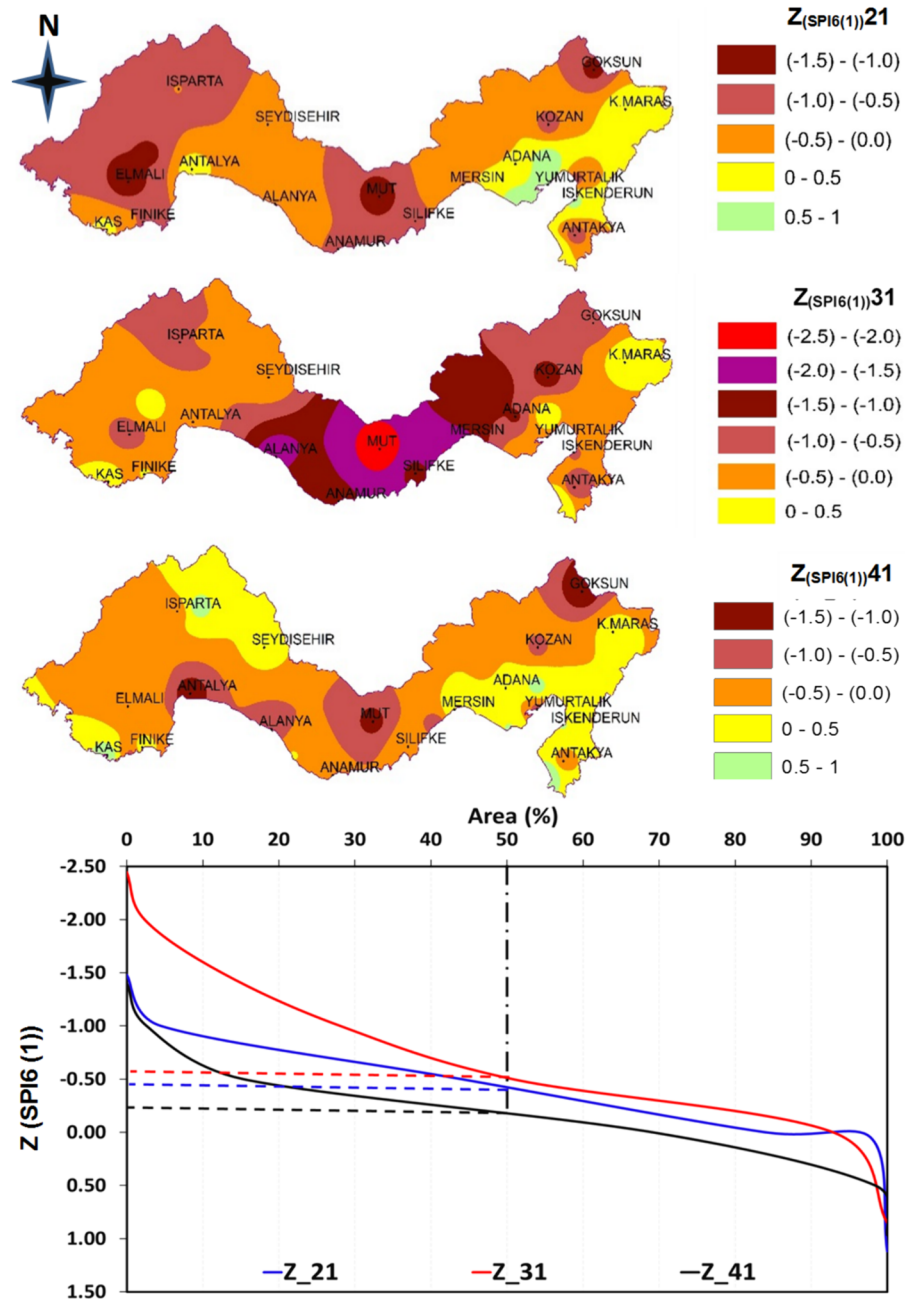


map shown in Fig. 5, when 50% of the basin area is taken into consideration for the trends in different time scales seen in the hypsometric curves, it is determined that there is a trend from the MIW climate class to the MID class in the central part of the basin. It is predicted that MIW and MID climate classes will maintain their dominance in the future.

Mann–Kendall trend maps and hypsometric curves of the SPI6 (1) season at the different time scales are presented in Fig. 10. For the SPI6 (1)

season at the 21-year time scale ($Z_{(SPI6(1))21}$), no significant trends were observed in either increasing or decreasing directions (within -1.96 to 1.96) across the entire study region. However, in the western part of the region, around Elmalı, in the central area around Mut, and in the eastern part around Gökşun, it is suggested to consider decreasing trends within $Z = (-1.5 - (-1.0))$. At the 31-year time scale, significant trends ($Z \geq -1.96$) were observed in Alanya, Mut, Silifke, and the surrounding areas,

Fig. 10 Mann–Kendall trend maps and hypsometric curves of SPI6 (1) at different time scales

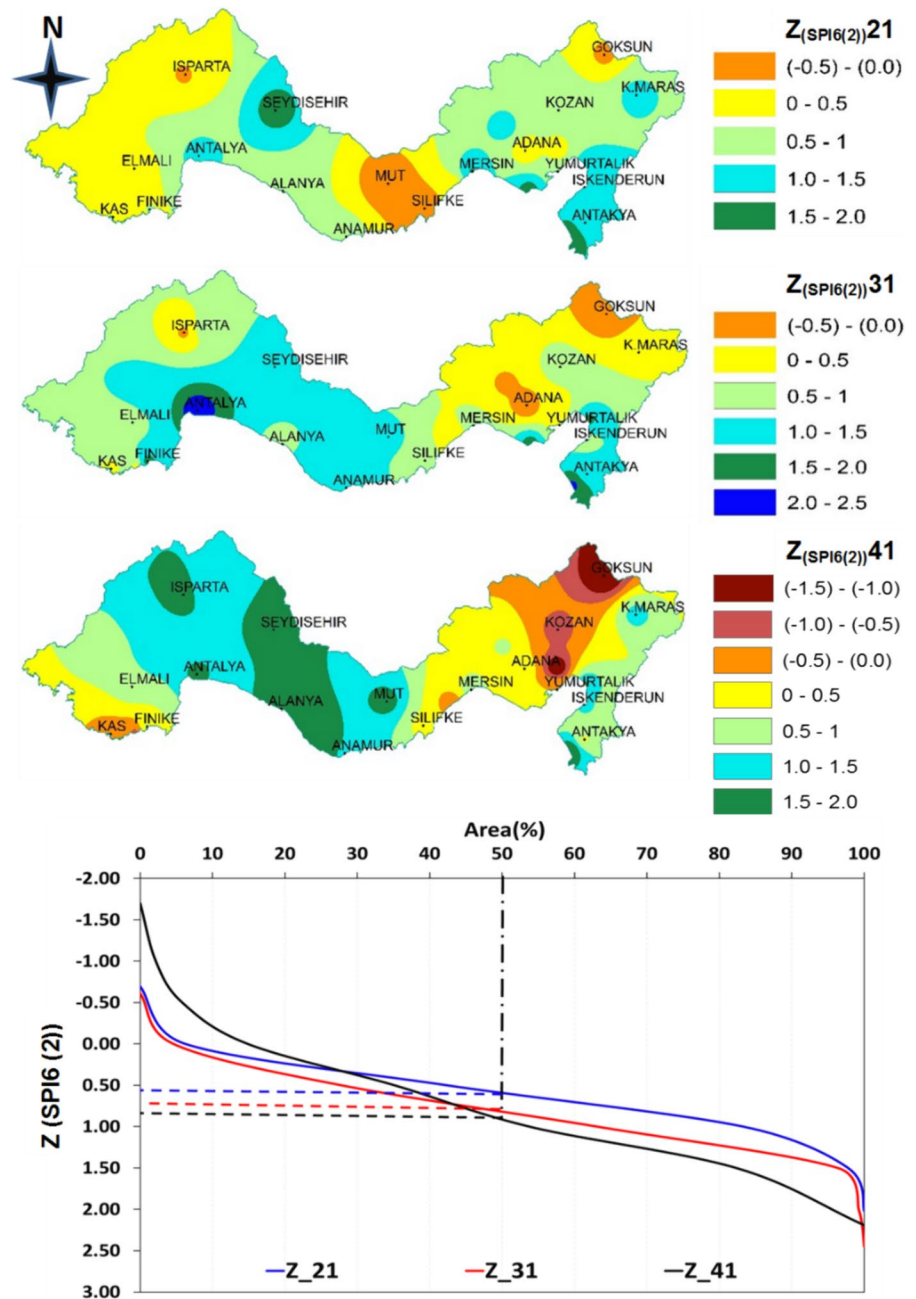


with a decreasing trend across the region. Considering the 41-year time scale, no significant trends were observed in increasing and decreasing directions across the area. Similar to the 21-year time scale, it was observed that the decreasing trends in the middle part of the region around Mut station stabilized. The presence of decreasing trends around the Mut station was confirmed. In the hypsometric curves, when

considering 50% of the region area, Z values were below -0.4 for the 21-year scale, below -0.6 for the 31-year scale, and below -0.25 for the 41-year scale. Despite not being statistically significant, decreasing-decreasing-decreasing trends persisted across all time scales in consecutive and overlapping intervals.

For the SPI6 (1) season at the 21-, 31-, and 41-year time scales, significant trends in the decreasing

Fig. 11 Mann–Kendall trend maps and hypsometric curves of SPI6 (2) at different time scales

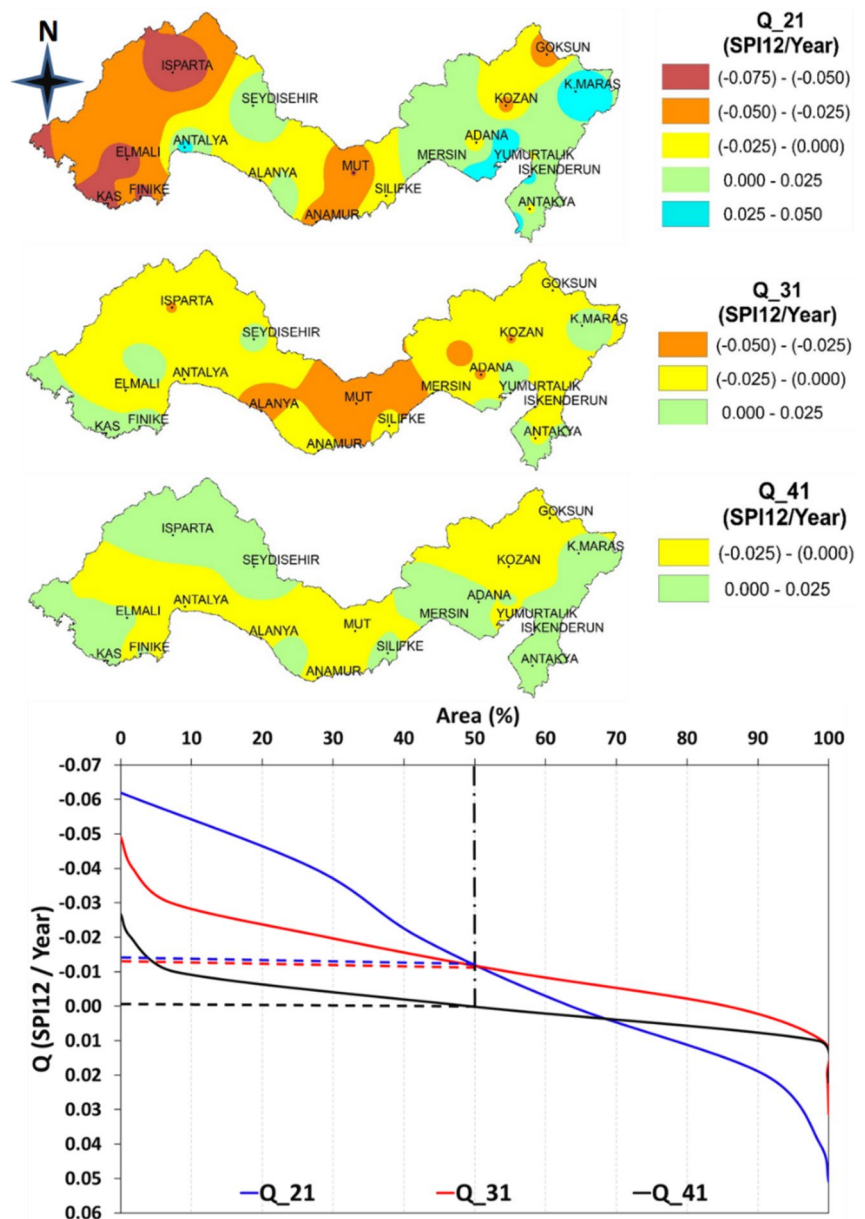


direction ($Z \leq -1.96$) were observed only at the 31-year time scale across the entire region. This pattern is similar to the SPI12 period. Mainly, a significant trend in the middle part of the region, around Mut station, from the MIW drought class toward the MID drought class was notable according to the drought class map shown in Fig. 5. Considering the spatial averages of the hypsometric curves, it is

anticipated that the MIW and MID drought classes will maintain their dominance in the future across the entire region, with a nonsignificant yet apparent trend toward the MID class.

Figure 11 shows Mann–Kendall trend maps and hypsometric curves of SPI6 (1) season at different time scales. The most notable observation for the SPI6 (2) period at the 21-year time scale was the

Fig. 12 Sen’s slope trend maps and hypsometric curves of SPI12 at different time scales



prevalent increasing trends across the region. Insignificant decreasing trends were observed around Mut and Silifke. In the subsequent decade, at the 31-year time scale, statistically significant trends appeared in Finike, Elmali, Seydisehir, Anamur, and Mut. In the region’s eastern part, a decrease in increasing trends was noted compared to the 21-year time scale. At the 41-year time scale, increasing trends gained importance in the western and central regions, while in the east, especially around Mersin, Adana, Kozan, and

Goksun, trends shifted toward a decreasing direction ($Z=(0-(-1.5))$). Considering 50% of the region part in the hypsometric curves, the Z statistic was below $Z\leq 0.55$ for the 21-year scale, $Z\leq 0.70$ in the subsequent decade, and $Z\leq 0.80$ at the 41-year scale. Despite being statistically insignificant, increasing-increasing-increasing trends persisted across all time scales.

In the SPI6 (2) season at the 21-, 31-, and 41-year scales, a prevailing trend of increasing trends in the region was identified, indicating a nonsignificant

tendency toward wetter conditions. According to the drought class map shown in Fig. 5, there was a nonsignificant trend from the MID drought class toward the MIW drought class across the entire region. Considering the spatial averages of the hypsometric curves, it is anticipated that the MIW and MID drought classes will maintain their dominance in the whole area in the future.

Sen's slope trend maps

Sen's slope (Q) statistics were obtained for the SPI12, SPI6 (1), and SPI6 (2) seasons at 21-, 31-, and 41-year time scales to determine the spatial distribution and hypsometric curves of meteorological drought in the region. In the SPI12 season, the spatial and temporal distribution of Q statistics in the Mediterranean region for all time scales is shown in Fig. 12. The linear modeling of trends using Sen's slope method has revealed changes in time scales more explicitly than MK maps in determining the spatial and temporal spread of meteorological drought in the region. The Sen's slope trend map and median-based drought class maps shown in Fig. 5 were jointly evaluated for this purpose.

In the SPI12 season at the 21-year time scale, the decreasing trends in the region occurred with speeds (SPI12/year) in the range of -0.025 – (-0.075) in the western areas of Isparta, Elmalı, Finike, Kaş, Mut, and Göksun. In the east, predominantly increasing trends were observed, with increasing annual trend speeds ranging from 0.000 to 0.050. At the 31-year time scale, it was determined that the decreasing trend speeds continued to slow down across the region. At the 41-year time scale, it was observed that decreasing trends persisted, and increasing trends spread across the area. Considering 50% of the region part in the hypsometric curves, the trend speeds were below $Q \leq -0.015$ SPI12/year, $Q \leq -0.014$ SPI12/year, and $Q \leq 0.001$ SPI12/year for the 21-, 31-, and 41-year time scales, respectively.

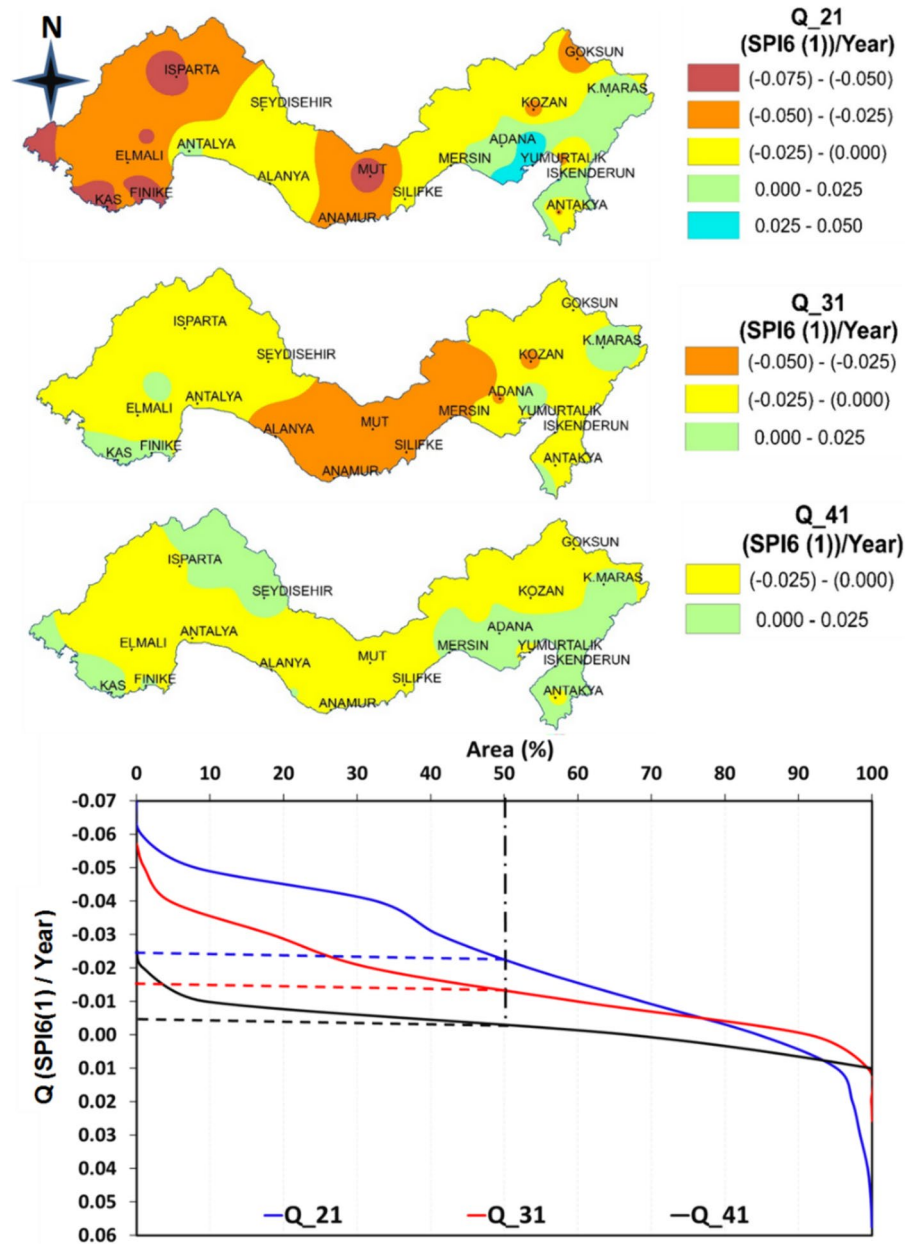
When considering the hypsometric curves of the SPI12 season, there was no significant difference in the drought spread rate in overlapping every 10 (31 years) years compared to the 21-year time scale. However, in the overlapping 10 (41 years) years, it was determined that the drought spread rate in the region slowed down and exhibited an increasing trend. Considering the drought class map given in Fig. 5, it is anticipated that in the future, there will be a trend toward the MID drought class shifting toward the MIW drought class in the region.

Sen's slope trend maps and hypsometric curves obtained for the SPI6 (1) season at different time scales are shown in Fig. 13. In the SPI6 (1) season, the trend speeds (SPI6 (1)/year) of decreasing and increasing trends that occurred in the region at the 21-year time scale were similar to the SPI12 season (-0.025 – (-0.075) ; 0.000–0.050). At the 31- and 41-year time scales, it was determined that the slowing down of decreasing trend speeds across the region exhibited the same behavior as the transitions between drought classes in the SPI12 season. In the hypsometric curves for the SPI6 (1) season, considering 50% of the region, the trend speeds were below $Q \leq -0.024$ SPI12/year, $Q \leq -0.016$ SPI12/year, and $Q \leq -0.005$ SPI6 (1)/year for the 21-, 31-, and 41-year time scales, respectively. It was observed that drought prevailed with decreasing, decreasing, and decreasing trends, but the spread rate slowed.

Considering the hypsometric curves of the 21-year time scale in the SPI6 (1) season, it was determined that drought spread exhibited decreasing trends in the region during overlapping and successive 31 (10 years) and 41 (10 years) periods. However, the speed gradually slowed down. When considering the drought class map given in Fig. 5, it is anticipated that in the future, there will be a trend toward the MID drought class shifting toward the MIW drought class in the study region, similar to the SPI12 season.

In Fig. 14, Sen's slope trend maps and hypsometric curves of SPI6 (1) season at different time scales are presented. In the SPI6 (2) season, at the 21-year time scale, the trend speeds (SPI6 (2)/year) of decreasing trends that occurred in the region in the west in the Isparta, Mut, and Göksun regions ranged from -0.025 to 0.000. Predominantly increasing trends (0.000–0.100) were observed in the east. At the 31-year time scale, it was determined that region-wide decreasing trend speeds did not change (-0.025 to 0.000), and their areal spreads declined. Increased trend speeds slowed (0.000–0.050), but their spreads expanded. In the 41-year time scale, it was found that the decreasing trend speeds did not change, but their spread expanded in the area covering Kozan, Adana, and Göksun. Increased trends spread across the entire region, but no change in trend speeds was observed. When considering 50% of the whole area in the hypsometric curves, it was determined that the trend speeds were below $Q \leq 0.024$ SPI6 (2)/year, $Q \leq 0.016$ SPI6 (2)/year,

Fig. 13 Sen's slope trend maps and hypsometric curves of SPI6 (1) season at different time scales



and $Q \leq 0.008$ SPI6 (2)/year for the 21-, 31-, and 41-year time scales, respectively. It was observed that trends were increasing, increasing, and increasing for three scales, indicating the dominance of moisture, but the spread rate slowed down.

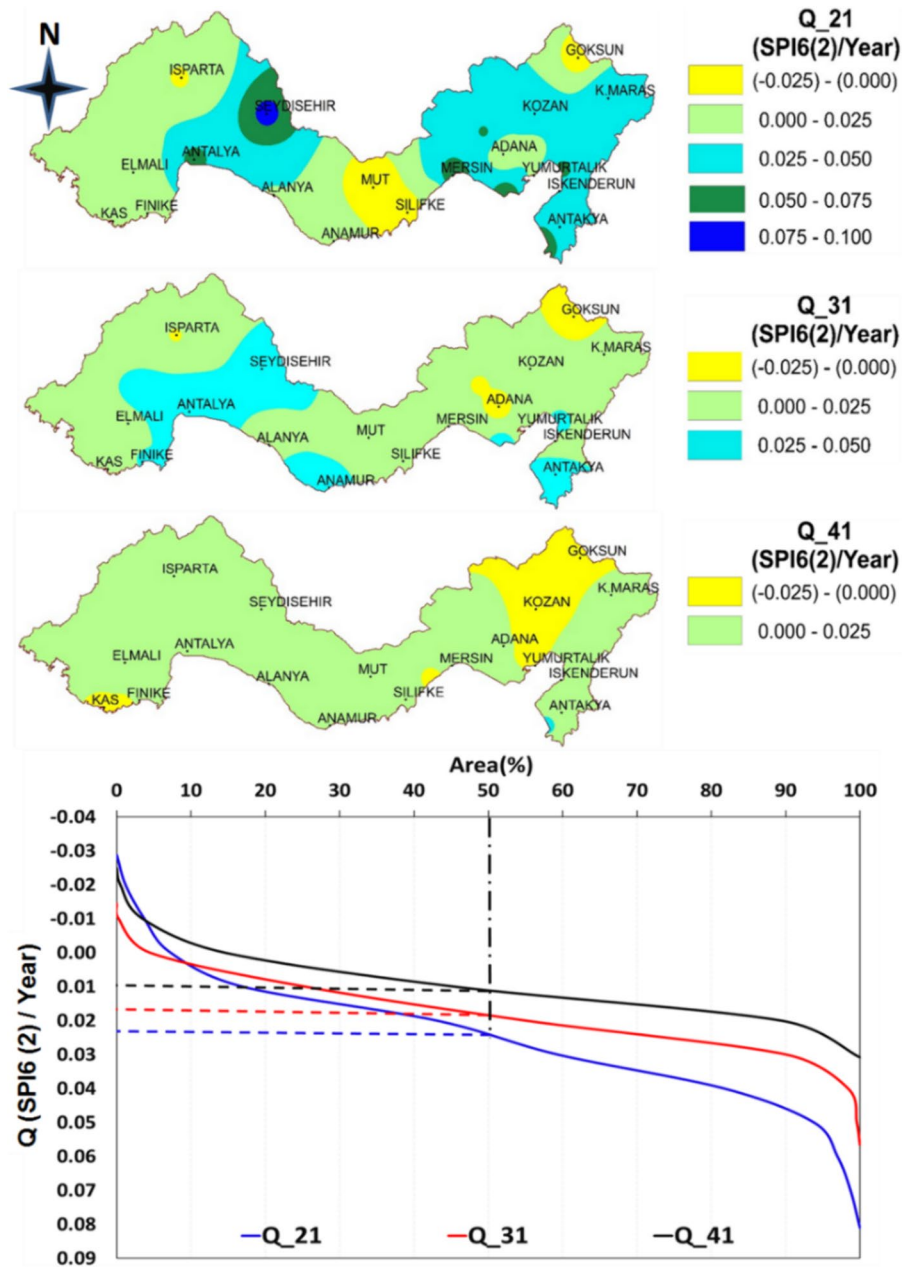
From the hypsometric curves of the SPI6 (2) season, it was determined that in overlapping 21-, 31-, and 41-year time scales, the increasing trends indicating increased moisture in the region showed a progressively slowing spread rate. Considering that the

drought class map is shown in Fig. 5, it is anticipated that in the future, the MIW drought class will maintain its dominant characteristic in the region.

Discussion

Gül and Kuzucu (2017) analyzed the meteorological drought of the Seyhan Basin in the eastern part of the study area using two different methods and

Fig. 14 Sen's slope trend maps and hypsometric curves of SPI6 (2) at different time scales



conducted a trend analysis. The study found no significant trend in monthly precipitation data but identified a noticeable decreasing trend in drought index values. Additionally, drought intensity and frequency have increased in recent years. Gumus (2019) determined the trend and trend start years of meteorological parameters measured at 14 stations in the Ceyhan and Seyhan basins. It was determined that there were significant temperature increases, and the trend

generally started in the mid-1990s. Simsek (2021) analyzed the hydrological drought of the Mediterranean region in 3-, 6-, and 12-month periods. As a result of the study, it was reported that ED and SD drought classes occurred at a higher rate in the central part of the region than in other parts of the region. In this study, a similar situation occurred in meteorological drought, especially for the SPI12 season, on time scales of 21 and 41 years. Dikici and Aksel (2021)

analyzed drought risk in the Ceyhan Basin using meteorological, hydrological, and hydrogeological data. These values were compared by determining the indices and indicators found in past studies, and their relationships were examined. It was reported that a slowly progressing drought occurred in the basin during the examined period. Precipitation in the basin has decreased over the last 50 years. It has been determined that drought occurrence is at serious levels in 20-year recurrence periods. Bayer Altin and Altin (2021) analyzed meteorological and hydrological drought using the values measured between 1967 and 2017 at flow and precipitation observation stations in the Eastern Mediterranean basin. In the study, meteorological drought was calculated with SPI and hydrological drought with a standardized streamflow index (SSI). As a result of the study, they reported that there was a 1-year delay between meteorological drought and hydrological drought according to the Pearson correlation coefficient. According to SPI 12, drought occurrence was quite evident between 2002–2003 and 2008–2009. This situation parallels the consecutive and overlapping time scale drought results of the SPI12 season 1978–2008/31 years for the central part of the study area. Gumus et al. (2022b) determined the trend of monthly total flow data measured between 1977 and 2015 at 20 flow observation stations in the Mediterranean region with MK, innovative polygon trend analysis (IPTA) and innovative trend significance test (ITST), the trend magnitude was determined with the SS method. From the results obtained, statistically decreasing series for the MK, ITST, and IPTA methods were determined in 55, 158, and 158 of the 240-time series, respectively, in the study region. Additionally, the average SS value at stations in the region's east was determined to be $-26\%/decade$. This result is quite similar to the spatial variation of SS values at all successive time scales of SPI12 and SPI6 (1) in the presented study, showing that the decrease in precipitation affects river flows and water resources. Gumus (2023) used temperature and precipitation data measured continuously for 51 years at 199 stations to analyze the drought of all of Turkey with the SPEI and SPI methods. The occurrence percentages of different drought classes for the Mediterranean region were evaluated spatially and temporally in the study where meteorological drought was examined in 3-, 6-, and 12-month periods. It can be said that the spatial distributions of

the occurrence percentage of drought classes obtained by the SPI method are quite similar to the formation rates and spatial distributions of drought classes in the SPI12 season on a 41-year time scale in this study. Soyulu Pekpostalci et al. (2023) conducted a meteorological drought analysis using the SPI method based on precipitation data recorded between 1971 and 2021 at 35 meteorological observation stations in the Mediterranean region. They calculated SPI series for 3-, 6-, and 12-month periods to evaluate meteorological drought. The spatial occurrence of different drought classes at stations for these time scales was presented. The results obtained closely resemble this study's outcomes of a 41-year time scale. In both studies, it was observed that the percentage of occurrence of the ED drought class is significant in the central part of the study area and at the Göksun station, while the percentage of occurrence of the SD drought class is notably high in the western part of the region, and the MD drought class has a high occurrence percentage in the northwest of the region. Seker and Gumus (2022) made a future projection of the precipitation and temperature values of the Mediterranean Region. As a result of the study, it was determined that with the SSP5–8.5 scenario, precipitation in the southeastern and eastern parts of the region will decrease by an average of 33.4% between 2021 and 2100.

Considering these studies on the study region in the literature, it is understood that the SPI method is used in the drought analysis of meteorological drought, and the MK test and the SS test are used to determine the drought trend and magnitude trend, respectively. When these studies on the drought of the region were examined, it was determined that the data length was considered as a period, and in this study presented, it was determined that it was possible to evaluate the change of drought from the past to the present in more detail if cumulative drought analysis was revealed by taking into account different data record lengths. The spatial distribution of the occurrence rate, trend, and change of different drought classes and hypsometric curves of the MK and Sen's slope statistics was evaluated in SPI12, SPI6 (1), and SPI6 (2) for data record lengths of 21, 31, and 41 years. From the results obtained as a result of the study and the results of previous studies, it was determined that the meteorological and hydrological drought risk is relatively high both in the central part of the study area and in the northeastern region (the southern part of the

Seyhan basin). From the spatial and temporal changes of the SPI 12 and SPI 6(2) values obtained in the 21-, 31-, and 41-year periods of the study region, drought increased in the region from 21- to 31-year and from 21- and 41-year data sets, while drought decreased in the analysis based on the 31- and 41-year data sets. In the SPI 6 (1) season, there is a decrease in the percentage of drought occurrence for each period of 10 years (21 to 31, 31 to 41, 21 to 41). For all seasons examined, it is seen that the magnitude of the SS value decreases with increasing data record length. In the central part of the region (around Mut station), a statistically significant decreasing trend was obtained with MK on a 31-month time scale in the SPI 12 and SPI6 (1) seasons. In SPI6 (2), no statistically significant increasing or decreasing trend exists in any data record length.

In the SPI12, SPI6 (1), and SPI6 (2) seasons, inverse correlations were identified between EW-ED, SW-SD, MW-MD, and MIW-MID drought classes across 21–31, 31–41, and 21–41-year scales. Comparing the formations of drought classes in the SPI12, SPI6 (1), and SPI6 (2) seasons across 21–31, 31–41, and 21–41-year time scales, it was determined that the absolute variability of the formations of EW, SW, ED, and SD drought classes in both increases and decreases was much greater than the absolute variability of the increases and decreases in MW, MIW, MID, and MD drought classes. This result coincides with the occurrence of floods and flooding events in the region in recent years. The results obtained should be considered in terms of improving the stream beds, increasing their capacity by evaluating the flood risk, and planning the existing water resources in drought due to the increase in the indices values of extreme drought and wet in the region. In addition, it is known that the productivity of agricultural activities in the Mediterranean region is affected by rainfall decreases and extreme rains and hailstorms, which seriously damage the region's economy.

Conclusion

This study aims to evaluate meteorological drought in the Mediterranean Region, which forms the southern borders of Turkey and is very sensitive to ocean oscillations across different time scales. Within the

scope of the study, monthly total precipitation records spanning 41 years were divided into the hydrological years 1978–1998 (21 years), 1978–2008 (31 years), and 1978–2018 (41 years) to obtain monthly SPI12, SPI6 (1), and SPI6 (2) seasons. Various drought class maps, drought class average formation maps, Mann–Kendall trend maps, and Sen's slope trend maps were obtained for different periods and time scales. The results of the study can be summarized as follows:

- Although there was no significant change in the average annual total precipitation data measured at 21, 31, and 41 years of recording periods, it was determined that data recording lengths were effective on meteorological drought results.
- As the length of the data record increases, the upper and lower bounds of the internal dependence become narrower, and the number of stations with internal dependence effect decreases from SPI12 to SPI6 (1 and 2).
- The region's extreme wet and drought formations are not stationary compared to other subclasses and carry risk.
- Statistically significant decreasing trends are evident in the central part of the study area over a data length of 31 years. It is understood that this part is the riskiest region regarding drought.
- Although SS and MK test statistics are similar spatially and temporally, the SS test revealed the transitions in drought changes more clearly.
- The predominance of MID and MIW periods throughout the region in the 41 years reveals that the region may experience hydrological drought in the coming years.

From the results obtained as a result of the study and the results of previous studies, it was determined that the meteorological and hydrological drought risk is relatively high both in the central part of the study area and in the northeastern region (the southern part of the Seyhan basin). The results obtained should be considered in terms of improving the stream beds, increasing their capacity by evaluating the flood risk, and planning the existing water resources in case of drought due to the increase in the index values of extreme drought and rainy periods in the region. It is possible to evaluate the impact of climate change on drought classes in drought studies that take into account consecutive and

overlapping data record lengths. In future studies, issues such as examining the effects of atmospheric oscillations on the meteorological and hydrological droughts of the region and considering the hydrological drought in the region can be addressed similarly to this presented study. The limitation of this study is that only the precipitation-based SPI method is taken into account in the evaluation of meteorological drought and that other methods that use potential evapotranspiration (PET) values in drought analysis in addition to the precipitation parameter are not used, considering that atmospheric oscillations will change temperatures in the region.

Acknowledgements The authors are thankful to the Turkish State Meteorological Service for providing the dataset.

Author contribution Ali Demir Keskiner and Oguz Simsek; analysis, conceptualization, methodology, writing.

Data availability All data generated or analyzed during this study are included in this manuscript.

Declarations

Ethics approval Not applicable.

Consent to participate Not applicable.

Consent for publication Not applicable.

Competing interests The authors declare no competing interests.

References

- Achite, M., Caloiero, T., Toubal, A. K. (2022). Rainfall and runoff trend analysis in the Wadi Mina Basin (Northern Algeria) using non-parametric tests and the ITA method. *Sustainability*, *14*. <https://doi.org/10.3390/su14169892>
- Achite, M., Simsek, O., Adarsh, S., Hartani, T., Caloiero, T. (2023). Assessment and monitoring of meteorological and hydrological drought in semiarid regions: The Wadi Ouahane basin case study (Algeria). *Physics and Chemistry of the Earth, Parts A/B/C*, *130*. <https://doi.org/10.1016/j.pce.2023.103386>
- Alsenjar, O., Aksu, H., & Çetin, M. (2022). The use of some specific drought indices to evaluate meteorological drought events in the Black Sea Region of Turkey. *Çukurova Tarım Ve Gıda Bilimleri Dergisi*, *37*, 261–272.
- Amiri, M. A., & Gocic, M. (2023). Analysis of temporal and spatial variations of drought over Serbia by investigating the applicability of precipitation-based drought indices. *Theoretical and Applied Climatology*, *154*, 261–274. <https://doi.org/10.1007/s00704-023-04554-6>
- Angelidis, P., Maris, F., Kotsovinos, N., & Hrissanthou, V. (2012). Computation of drought index SPI with alternative distribution functions. *Water Resources Management*, *26*, 2453–2473. <https://doi.org/10.1007/s11269-012-0026-0>
- Balram, P., Fanai, L. (2021). Meteorological drought assessment using standardized precipitation index for different agro-climatic zones of Odisha. *Mausam*, *71*:467–480. <https://doi.org/10.54302/mausam.v71i3.48>
- Barriopedro, D., Fischer, E. M., Luterbacher, J., Trigo, R. M., & García-Herrera, R. (2011). The hot summer of 2010: Redrawing the temperature record map of Europe. *Science*, *332*, 220–224. <https://doi.org/10.1126/science.1201224>
- Basakin, E. E., Ozger, M., & Unal, N. E. (2019). Gri Tahmin Yöntemi İle İstanbul Su Tüketiminin Modellenmesi. *Politeknik Dergisi*, *22*, 755–761. <https://doi.org/10.2339/politeknik.422727>
- Bayer Altın, T., & Altın, B. N. (2021). Response of hydrological drought to meteorological drought in the eastern Mediterranean Basin of Turkey. *Journal of Arid Land*, *13*, 470–486. <https://doi.org/10.1007/s40333-021-0064-7>
- Bazrafshan, O., Zamani, H., Mozaffari, E., Azhdari, Z., Shekari, M. (2023). Trivariate risk analysis of meteorological drought in Iran under climate change scenarios. *Meteorology and Atmospheric Physics*, *135*. <https://doi.org/10.1007/s00703-023-00988-9>
- Berhail, S., & Katipoğlu, O. M. (2023). Comparison of the SPI and SPEI as drought assessment tools in a semi-arid region: Case of the Wadi Mekerra basin (northwest of Algeria). *Theoretical and Applied Climatology*, *154*, 1373–1393. <https://doi.org/10.1007/s00704-023-04601-2>
- Buyukyildiz, M. (2022). Evaluation of annual total precipitation in the transboundary Euphrates-Tigris River Basin of Türkiye using innovative graphical and statistical trend approaches. *Applied Water Science*, *13*. <https://doi.org/10.1007/s13201-022-01845-7>
- Caloiero, T. (2017). Drought analysis in New Zealand using the standardized precipitation index. *Environmental Earth Sciences*, *76*. <https://doi.org/10.1007/s12665-017-6909-x>
- Carter, T. G., et al. (1972). A new bathymetric chart and physiography of the Mediterranean Sea. In D. J. Stanley (Ed.), *The Mediterranean sea: A natural sedimentation laboratory* (pp. 1–23). Dowden, Hutchinson and Ross Pennsylvania.
- Citakoglu, H., & Coşkun, Ö. (2022). Comparison of hybrid machine learning methods for the prediction of short-term meteorological droughts of Sakarya Meteorological Station in Turkey. *Environmental Science and Pollution Research*, *29*, 75487–75511. <https://doi.org/10.1007/s11356-022-21083-3>
- Citakoglu, H., & Minarecioglu, N. (2021). Trend analysis and change point determination for hydro-meteorological and groundwater data of Kizilirmak basin. *Theoretical and Applied Climatology*, *145*, 1275–1292. <https://doi.org/10.1007/s00704-021-03696-9>
- Dai, M., et al. (2022). Propagation characteristics and mechanism from meteorological to agricultural drought in various seasons. *Journal of Hydrology*, *610*. <https://doi.org/10.1016/j.jhydrol.2022.127897>
- Dikici, M. (2020). Drought analysis with different indices for the Asi Basin (Turkey). *Scientific Reports*, *10*. <https://doi.org/10.1038/s41598-020-77827-z>

- Dikici, M., Aksel, M. (2021). Comparison of drought indices in the case of the Ceyhan Basin. *International Journal of Environment and Geoinformatics*, 8:113–125. <https://doi.org/10.30897/ijegeo.792379>
- Dukat, P., Bednorz, E., Ziemlińska, K., Urbaniak, M. (2022). Trends in drought occurrence and severity at mid-latitude European stations (1951–2015) estimated using standardized precipitation (SPI) and precipitation and evapotranspiration (SPEI) indices. *Meteorology and Atmospheric Physics*, 134. <https://doi.org/10.1007/s00703-022-00858-w>
- Esit, M. (2023). Investigation of innovative trend approaches (ITA with significance test and IPTA) comparing to the classical trend method of monthly and annual hydrometeorological variables: A case study of Ankara region, Turkey. *Journal of Water and Climate Change*, 14, 305–329. <https://doi.org/10.2166/wcc.2022.356>
- Esit, M., Çelik, R., Akbas, E. (2023a). Long-term meteorological and hydrological drought characteristics on the lower Tigris-Euphrates basin, Türkiye: Relation, impact and trend. *Environmental Earth Sciences*, 82. <https://doi.org/10.1007/s12665-023-11182-w>
- Esit, M., Çelik, R., & Akbas, E. (2023b). Spatial and temporal variation of meteorological parameters in the lower Tigris-Euphrates basin, Türkiye: Application of non-parametric methods and an innovative trend approach. *Water Science & Technology*, 87, 1982–2004. <https://doi.org/10.2166/wst.2023.116>
- Esit, M., Yuce, M. I., Deger, İ. H., Yasa, I. (2023c). Trend and variability analysis in rainfall and temperature records over Van Province, Türkiye. *Theoretical and Applied Climatology*. <https://doi.org/10.1007/s00704-023-04644-5>
- Giorgi, F. (2006). Climate change hot-spots. *Geophysical Research Letters*, 33. <https://doi.org/10.1029/2006gl025734>
- Gocic, M., & Trajkovic, S. (2013). Analysis of changes in meteorological variables using Mann-Kendall and Sen's slope estimator statistical tests in Serbia. *Global and Planetary Change*, 100, 172–182. <https://doi.org/10.1016/j.gloplacha.2012.10.014>
- Gül, G. O., & Kuzucu, A. (2017). Analysis of drought severity in Seyhan river basin. *European Water*, 60, 211–217.
- Gumus, V. (2019). Spatio-temporal precipitation and temperature trend analysis of the Seyhan-Ceyhan River Basins, Turkey. *Meteorological Applications*, 26, 369–384. <https://doi.org/10.1002/met.1768>
- Gumus, V. (2023). Evaluating the effect of the SPI and SPEI methods on drought monitoring over Turkey. *Journal of Hydrology*, 626. <https://doi.org/10.1016/j.jhydrol.2023.130386>
- Gumus, V., Simsek, O., Avsaroglu, Y., & Agun, B. (2021). Spatio-temporal trend analysis of drought in the GAP Region, Turkey. *Natural Hazards*, 109, 1759–1776. <https://doi.org/10.1007/s11069-021-04897-1>
- Gumus, V., Avsaroglu, Y., Simsek, O. (2022a). Streamflow trends in the Tigris river basin using Mann-Kendall and innovative trend analysis methods. *Journal of Earth System Science*, 131. <https://doi.org/10.1007/s12040-021-01770-4>
- Gumus, V., Simsek, O., & Avsaroglu, Y. (2022b). Evaluation of long-term monthly mean streamflow trend in the Mediterranean basins using different methods. *Theoretical and Applied Climatology*, 151, 1369–1382. <https://doi.org/10.1007/s00704-022-04293-0>
- Gümüş, V., Avşaroğlu, Y., Şimşek, O., Doğan Dinsever, L. (2023). Evaluation of meteorological time series trends in Southeastern Anatolia, Turkey. *Geofizika*, 40:51–73. <https://doi.org/10.15233/gfz.2023.40.3>
- Gumus, V., Dinsever, L. D., & Avsaroglu, Y. (2023). Analysis of drought characteristics and trends during 1965–2020 in the Tigris River basin, Turkey. *Theoretical and Applied Climatology*, 151, 1871–1887. <https://doi.org/10.1007/s00704-023-04363-x>
- Haile, G. G., Tang, Q., Li, W., Liu, X., Zhang, X. (2019). Drought: Progress in broadening its understanding. *WIREs Water*, 7. <https://doi.org/10.1002/wat2.1407>
- Handmer, J., et al. (2012). Changes in impacts of climate extremes: human systems and ecosystems. In C. B. Field, V. Barros, T. F. Stocker, D. Qin, D. J. Dokken, K. L. Ebi, M. D. Mastrandrea, K. J. Mach, G.-K. Plattner, S. K. Allen, M. Tignor, & P. M. Midgley (Eds.), *Managing the risks of extreme events and disasters to advance climate change adaptation. A Special Report of Working Groups I and II of the Intergovernmental Panel on Climate Change (IPCC)* (pp. 231–290). Cambridge University Press.
- Hinis, M. A., Geyikli, M. S., & Qin, A. (2023). Accuracy evaluation of standardized precipitation index (SPI) estimation under conventional assumption in Yeşilirmak, Kızılırmak, and Konya Closed Basins, Turkey. *Advances in Meteorology*, 2023, 1–13. <https://doi.org/10.1155/2023/5142965>
- Hirabayashi, Y., Kanae, S., Emori, S., Oki, T., & Kimoto, M. (2010). Global projections of changing risks of floods and droughts in a changing climate. *Hydrological Sciences Journal*, 53, 754–772. <https://doi.org/10.1623/hysj.53.4.754>
- Intergovernmental Panel on Climate Change (IPCC). (2020). *Climate Change and Land*. An IPCC Special Report on climate change, desertification, land degradation, sustainable land management, food security, and greenhouse gas fluxes in terrestrial ecosystems; Summary for Policymakers.
- Karavitis, C. A., Alexandris, S., Tsesmelis, D. E., & Athanopoulos, G. (2011). Application of the standardized precipitation index (SPI) in Greece. *Water*, 3, 787–805. <https://doi.org/10.3390/w3030787>
- Karimi, M., Melesse, A. M., Khosravi, K., Mamuye, M., & Zhang, J. (2019). Analysis and prediction of meteorological drought using SPI index and ARIMA model in the Karkheh River Basin, Iran. In: *Extreme Hydrology and Climate Variability*, pp 343–353. <https://doi.org/10.1016/b978-0-12-815998-9.00026-9>
- Kartal, V. (2023). Assessment of drought using different tests and drought indices in Elazığ, Turkey. *Water Science & Technology*, 88, 1767–1794. <https://doi.org/10.2166/wst.2023.315>
- Kaur, N., Yousuf, A., & Singh, M. (2021). Long term rainfall variability and trend analysis in lower Shivaliks of Punjab, India. *Mausam*, 72, 571–582.
- Keskiner, A. D., & Cetin, M. (2023). Kuraklık Gidiş ve Büyüklüğünün Zaman ve Mekan Boyutunda Belirlenmesi: Güneydoğu Anadolu Projesi (GAP) Alanında Bir

- Uygulama. *Politeknik Dergisi*, 26, 1079–1089. <https://doi.org/10.2339/politeknik.1000596>
- Keskiner, A. D., Cetin, M., Simsek, M., Akin, S. (2020). Kuraklık Riski Altındaki Havzalarda Gölet Haznelerinin Tasarımı: Seyhan Havzasında Bir Uygulama. *Teknik Dergi*, 31:10189–10210. <https://doi.org/10.18400/tekderg.505584>.
- Kiem, A. S., et al. (2016). Natural hazards in Australia: Droughts. *Climatic Change*, 139, 37–54. <https://doi.org/10.1007/s10584-016-1798-7>
- Kuba, E. B., Deniz, Z. A., & Öztürk, B. Türkiye’de 1960-2010 döneminde oluşan sıcak hava dalgalarının klimatolojik ve meteorolojik analizi. Paper presented at the *TÜCAUM International Geography Symposium*.
- Landau, S., & Everitt, B. S. (2003). *A Handbook of Statistical Analyses Using SPSS*. <https://doi.org/10.1201/9780203009765>
- Lettenmaier, D. P., Wood, E. F., & Wallis, J. R. (1994). Hydroclimatological trends in the continental United States, 1948–88. *Journal of Climate*, 7, 586–607. [https://doi.org/10.1175/1520-0442\(1994\)007%3c0586:Hctitc%3e2.0.Co;2](https://doi.org/10.1175/1520-0442(1994)007%3c0586:Hctitc%3e2.0.Co;2)
- Lin, H., Wang, J., Li, F., Xie, Y., Jiang, C., & Sun, L. (2020). Drought trends and the extreme drought frequency and characteristics under climate change based on SPI and HI in the upper and middle reaches of the Huai River Basin, China. *Water*. <https://doi.org/10.3390/w12041100>
- Liu, Z. N., Yu, X. Y., Jia, L. F., Wang, Y. S., Song, Y. C., & Meng, H. D. (2021). The influence of distance weight on the inverse distance weighted method for ore-grade estimation. *Scientific Reports*, 11. <https://doi.org/10.1038/s41598-021-82227-y>
- McKee, T. B., Doesken, N. J., & Kleist, J. (1993). The relationship of drought frequency and duration to time scales. Paper presented at the In: Proceedings of the 8th conference on applied climatology, Boston.
- Minarecioğlu, N., Çitakoğlu, H. (2019). Trend analysis of monthly average flows of Kizilirmak Basin. *Journal of Anatolian Environmental and Animal Sciences*, 4, 454–459. <https://doi.org/10.35229/jaes.595095>
- Modarres, R., Sarhadi, A., & Burn, D. H. (2016). Changes of extreme drought and flood events in Iran. *Global and Planetary Change*, 144, 67–81. <https://doi.org/10.1016/j.gloplacha.2016.07.008>
- Mohsin, T., & Gough, W. A. (2009). Trend analysis of long-term temperature time series in the Greater Toronto Area (GTA). *Theoretical and Applied Climatology*, 101, 311–327. <https://doi.org/10.1007/s00704-009-0214-x>
- Mujumdar, M., et al. (2020). Droughts and floods. In: *Assessment of Climate Change over the Indian Region*, pp 117–141. https://doi.org/10.1007/978-981-15-4327-2_6
- Nan, Y., Bao-hui, M., & Chun-kun, L. (2011). Impact analysis of climate change on water resources. *Procedia Engineering*, 24, 643–648. <https://doi.org/10.1016/j.proeng.2011.11.2710>
- Oguz, K., Akin, B. S. (2019). Doğu Akdeniz Havzasında Sıcaklık, Yağış ve Aerosol Değişiminin İncelenmesi. *Mühendislik Bilimleri ve Tasarım Dergisi*, 7, 244–253. <https://doi.org/10.21923/jesd.464737>
- Ozturk, T., Ceber, Z. P., Türkes, M., & Kurnaz, M. L. (2015). Projections of climate change in the Mediterranean Basin by using downscaled global climate model outputs. *International Journal of Climatology*, 35, 4276–4292. <https://doi.org/10.1002/joc.4285>
- Patel, N. R., Chopra, P., & Dadhwal, V. K. (2007). Analyzing spatial patterns of meteorological drought using standardized precipitation index. *Meteorological Applications*, 14, 329–336. <https://doi.org/10.1002/met.33>
- Ryan, B. F., Joiner, B. L., & Cryer, J. D. (2012). *Minitab Handbook: Updated for release 16* (6th ed.). Brooks/Cole Publishing Co.
- Salmi, T., Määttä, A., Anttila, P., Ruoho-Airola, T., & Amnell, T. (2002). Detecting trends of annual values of atmospheric pollutants by the Mann-Kendall test and Sen’s slope estimates MAKESENS—The excel template application. *Finish Meteorological Institute, Helsinki*.
- Saris, F. (2021). Türkiye’de Evsel Su Tedarik ve Tüketim İstatistiklerinin Değerlendirilmesi. *Coğrafi Bilimler Dergisi*, 19:195–216. <https://doi.org/10.33688/aucbd.883794>
- Schär, C., Vidale, P. L., Lüthi, D., Frei, C., Häberli, C., Liniger, M. A., & Appenzeller, C. (2004). The role of increasing temperature variability in European summer heatwaves. *Nature*, 427, 332–336. <https://doi.org/10.1038/nature02300>
- Seker, M., Gumus, V. (2022). Projection of temperature and precipitation in the Mediterranean region through multi-model ensemble from CMIP6. *Atmospheric Research*, 280. <https://doi.org/10.1016/j.atmosres.2022.106440>
- Sen, P. K. (1968). Estimates of the regression coefficient based on Kendall’s tau. *Journal of the American Statistical Association*, 63, 1379–1389. <https://doi.org/10.1080/01621459.1968.10480934>
- Sharafi, S., Ghaleini, M. M., Sadeghi, S. (2022). Spatial and temporal analysis of drought in various climates across Iran using the Standardized Precipitation Index (SPI). *Arabian Journal of Geosciences*, 15. <https://doi.org/10.1007/s12517-022-10489-5>
- Shifteh Some’e, B., Ezani, A., & Tabari, H. (2012). Spatiotemporal trends and change point of precipitation in Iran. *Atmospheric Research*, 113, 1–12. <https://doi.org/10.1016/j.atmosres.2012.04.016>
- Simsek, O. (2021). Hydrological drought analysis of Mediterranean basins, Turkey. *Arabian Journal of Geosciences*, 14. <https://doi.org/10.1007/s12517-021-08501-5>
- Simsek, O., Yildiz-Bozkurt, S., Gumus, V. (2023). Analysis of meteorological drought with different methods in the Black Sea region, Turkey. *Acta Geophysica*. <https://doi.org/10.1007/s11600-023-01099-0>
- Singh, V., Nema, A. K., Chouksey, A., Kar, S. K. (2022). Spatiotemporal evaluation of drought characteristics in south Bihar region using Standardized Precipitation Index (SPI). *Arabian Journal of Geosciences*, 15. <https://doi.org/10.1007/s12517-022-10473-z>
- Soylu Pekpostalci, D., Tur, R., & Danandeh Mehr, A. (2023). Spatiotemporal variations in meteorological drought across the Mediterranean region of Turkey. *Pure and Applied Geophysics*, 180, 3089–3104. <https://doi.org/10.1007/s00024-023-03312-z>
- Tallaksen, L. M., & Van Lanen, H. A. (2004). Hydrological drought: Processes and estimation methods for streamflow and groundwater.

- Thom, H. C. S. (1958). A note on the gamma distribution. *Monthly Weather Review*, 86, 117–122. [https://doi.org/10.1175/1520-0493\(1958\)086%3c0117:Anotgd%3e2.0.Co;2](https://doi.org/10.1175/1520-0493(1958)086%3c0117:Anotgd%3e2.0.Co;2)
- Thom, H. C. S. (1966). Some methods of climatological analysis. Secretariat of the World Meteorological Organization, Geneva.
- Topçu, E., & Karaçor, F. (2023). A comparative investigation on the applicability of the actual precipitation index (API) with the standardized precipitation index (SPI): The case study of Aras Basin, Turkey. *Theoretical and Applied Climatology*, 154, 29–42. <https://doi.org/10.1007/s00704-023-04499-w>
- Tsesmelis, D. E., Leveidioti, I., Karavitis, C. A., Kalogeropoulos, K., Vasilakou, C. G., Tsatsaris, A., Zervas, E. (2023). Spatiotemporal application of the standardized precipitation index (SPI) in the Eastern Mediterranean. *Climate*, 11. <https://doi.org/10.3390/cli11050095>
- Turkes, M. (2020). Climate and drought in Turkey. In: *Water Resources of Turkey*. World Water Resources. pp 85–125. https://doi.org/10.1007/978-3-030-11729-0_4
- Vivoni, E. R., Di Benedetto, F., Grimaldi, S., Eltahir, E. A. B. (2008). Hypsometric control on surface and subsurface runoff. *Water Resources Research*, 44. <https://doi.org/10.1029/2008wr006931>
- Wang, W., Ertsen, M. W., Svoboda, M. D., & Hafeez, M. (2016). Propagation of drought: From meteorological drought to agricultural and hydrological drought. *Advances in Meteorology*, 2016, 1–5. <https://doi.org/10.1155/2016/6547209>
- Wang, F., et al. (2020). Re-evaluation of the power of the Mann-Kendall test for detecting monotonic trends in hydrometeorological time series. *Frontiers in Earth Science*, 8. <https://doi.org/10.3389/feart.2020.00014>
- Wilhite, D. A. (2016). *Droughts: A global assessment*. Routledge.
- Wu, H., Soh, L.-K., Samal, A., & Chen, X.-H. (2007). Trend analysis of streamflow drought events in Nebraska. *Water Resources Management*, 22, 145–164. <https://doi.org/10.1007/s11269-006-9148-6>
- Ye, L., Shi, K., Zhang, H., Xin, Z., Hu, J., Zhang, C. (2019). Spatio-temporal analysis of drought indicated by SPEI over northeastern China. *Water*, 11. <https://doi.org/10.3390/w11050908>
- Yilmaz, A. G., Shanableh, A., Al-Ruzouq, R. I., Kayemah, N. (2020). Spatio-temporal trend analysis of groundwater levels in Sharjah, UAE. *International Journal of Environmental Science and Development*, 11, 9–14. <https://doi.org/10.18178/ijesd.2020.11.1.1218>
- Yue, S., & Wang, C. Y. (2002). Regional streamflow trend detection with consideration of both temporal and spatial correlation. *International Journal of Climatology*, 22, 933–946. <https://doi.org/10.1002/joc.781>

Publisher's Note Springer Nature remains neutral with regard to jurisdictional claims in published maps and institutional affiliations.

Springer Nature or its licensor (e.g. a society or other partner) holds exclusive rights to this article under a publishing agreement with the author(s) or other rightsholder(s); author self-archiving of the accepted manuscript version of this article is solely governed by the terms of such publishing agreement and applicable law.